

A new luminosity function for galaxies as given by the mass-luminosity relationship

Zaninetti Lorenzo

*Dipartimento di Fisica Generale, Via Pietro Giuria 1,
10125 Torino, Italy*

zaninetti@ph.unito.it

<http://www.ph.unito.it/~zaninetti>

ABSTRACT

The search for a luminosity function for galaxies both alternative or companion to a Schechter function is a key problem in the reduction of data from catalogs of galaxies. Two luminosity functions for galaxies can be built starting from two distributions of mass as given by the fragmentation. A first overall distribution function is the Kiang function that represents a useful description of the area and volume distribution of the Poisson Voronoi diagrams. The second distribution, that covers the case of low mass galaxies, is the truncated Pareto distribution : in this model we have a natural bound due to the minimum mass/luminosity observed and an upper bound (function of the considered environment) represented by the boundary with the observed mass/luminosity overall behaviour. The mass distribution is then converted into a luminosity distribution through a standard mass-luminosity relationship. The mathematical rules to convert the probability density function are used and the two new functions are normalised to the total number of galaxies per unit volume. The test of the two new luminosity functions for galaxies that cover different ranges in magnitude was made on the Sloan Digital Sky Survey (SDSS) in five different bands; the results are comparable to those of the Schechter function. A new parameter that indicates the stellar content is derived. The joint distribution in red-shift and flux , the mean red-shift and the number density connected with the first luminosity function for galaxies are obtained by analogy with the Schechter function. A new formula that allows us to express the mass as a function of the absolute magnitude is derived.

Subject headings: Galaxies: fundamental parameters — Galaxies: statistics — Galaxies: luminosity function, mass function

1. Introduction

Over the years the search for a luminosity function for galaxies has played a relevant role in the analysis of data from catalogs. A model for the luminosity of galaxies is the Schechter function

$$\Phi(L)dL = \left(\frac{\Phi^*}{L^*}\right)\left(\frac{L}{L^*}\right)^\alpha \exp\left(-\frac{L}{L^*}\right)dL \quad , \quad (1)$$

where α sets the slope for low values of L , L^* is the characteristic luminosity and Φ^* is the normalisation. This function was suggested by Schechter (1976) in order to substitute other analytical expressions, see for example formula (3) in Kiang (1961). Over the years this function has also been applied to describe physical quantities related to the optical luminosity , such as the CO luminosity for galaxies , Keres et al. (2003), and the barionic mass function of galaxies , Bell et al. (2003a).

An astronomical form of equation (1) can be deduced by introducing the distribution in absolute magnitude

$$\begin{aligned} \Phi(M)dM = & \quad (0.4\ln 10)\Phi^*10^{0.4(\alpha+1)(M^*-M)} \\ & \times \exp(-10^{0.4(M^*-M)})dM \quad , \end{aligned} \quad (2)$$

where M^* is the characteristic magnitude as derived from the data. This distribution has a maximum at

$$M_{p,max} = M^* - 1.085 \ln(\alpha + 1.0) \quad , \quad (3)$$

where p,max means position of the maximum. In approaching this value the function will progressively flatten.

At present this function is widely used and Table 1 reports , as an example , the parameters from three catalogs

- The 2dF Galaxy Redshift Survey (2dFGRS) based on a sample of 75589 galaxies, see first line of Table 3 in Madgwick et al. (2002).
- The r^* -band luminosity function for a sample of 147986 galaxies at $z = 0.1$ from the Sloan Digital Sky Survey (SDSS) , see Blanton et al. (2003).
- The galaxy luminosity function for a sample of 10095 galaxies from the Millennium Galaxy Catalogue (MGC) , see Driver et al. (2005).

Over the years many modifications have been made to the standard Schechter function in order to improve its fit: we report three of them. When the fit of the rich clusters

luminosity function is not satisfactory a two-component Schechter-like function is introduced , see Driver & Phillipps (1996). This two-component function is the Schechter function when $L_{Dwarf} < L < L_{max}$ and has $(\frac{L}{L_{Dwarf}})^{\alpha_{Dwarf}}$ dependence when $L_{min} < L < L_{Dwarf}$: L_{Dwarf} represents the magnitude where dwarfs first dominate over giants , α_{Dwarf} the faint slope parameter for the dwarf population , the index *min* and *max* denote the minimum and the maximum.

Another example is the hybrid Schechter+power-law fit to fit the faint-end of the K-band, see Bell et al. (2003b).

Another function introduced in order to fit the case of extremely low luminosity galaxies is the double Schechter function , see Blanton et al. (2005) , where the parameters Φ^* and α that characterise the Schechter function have been doubled in $\phi_{*,1}, \phi_{*,2}$ and α_1, α_2 . The previous efforts bring the attention toward two ranges in luminosity for galaxies : an overall zone from high luminosity to low luminosity and the low luminosity zone. This situation remembers the case of the stars in which three zones are considered , see Scalo (1986), Kroupa et al. (1993), and Binney & Merrifield (1998) ; in this case the range of existence of the zones as well as the exponent that characterises the power law behaviour are functions of the investigated environment. These three zones in the mass distribution of the stars have been investigated at the light of the physical processes in Elmegreen (2004); they correspond to brown dwarf masses $\approx 0.02\mathcal{M}_{\odot}$, to intermediate mass stars and high mass stars.

The starting point of this paper is a statistical distribution in the mass of the galaxies , \mathcal{M} as given by a standard gamma variate with a range of existence $0 < \mathcal{M} < \infty$. This distribution describes the area of the irregular Voronoi polygons. This distribution in mass can be converted in a new statistical distribution for the luminosity of galaxies through an analogy with the physics of the stars. This new distribution in luminosity , L , is characterised by a range of existence $0 < L < \infty$ and a local maximum , named mode. A second distribution in the masses starts from a truncated Pareto distribution , after Pareto (1896) , with a range of existence $\mathcal{M}_{min} < \mathcal{M} < \mathcal{M}_{max}$. The standard procedure of conversion from

Table 1: The parameters of the Schechter function from 2dFGRS , SDSS and MGC .

<i>parameter</i>	<i>2dFGRS</i>	<i>SDSS (r*) band</i>	<i>MGC</i>
$M^* [mags]$	-19.79 ± 0.04	-20.44 ± 0.01	-19.60 ± 0.04
α	-1.19 ± 0.01	-1.05 ± 0.01	-1.13 ± 0.02
$\Phi^* [h \text{ Mpc}^{-3}]$	$(1.59 \pm 0.1)10^{-2}$	$(1.49 \pm 0.04)10^{-2}$	$(1.77 \pm 0.15)10^{-2}$

from mass to luminosity allows us to derive a truncated Pareto type luminosity function that has a range of existence $L_{min} < L < L_{max}$. In this distribution the mode is at L_{min} .

Section 2.2 first introduces the 2D Voronoi diagrams and then describes the mathematical details that allow us to deduce two new physical functions for luminosity of galaxies and Section 3 reports a first test based on the SDSS photometric catalog.

In Section 4 the red-shift dependence of the Schechter function and the first new function are explored in detail. Section 5 reports the mass evaluation for galaxies based on the first luminosity function as well as a new formula for the limiting mass. Section 6 summarises the results.

2. From the mass to the magnitude

The first paragraph briefly introduces the 2D Voronoi diagrams as produced by two types of seeds. These two statistical distributions adopted to fit the area of the irregular Voronoi polygons can be taken as a starting point to construct two luminosity functions for galaxies.

2.1. The Voronoi Diagrams

When the seeds are randomly and uncorrelated distributed, are called Poisson Voronoi diagrams. A great number of natural phenomena are described by Poisson Voronoi diagrams, we cite some of them : lattices in quantum field theory, see Drouffe & Itzykson (1984); conductivity and percolation in granular composites, see Jerauld et al. (1984a) and Jerauld et al. (1984b); modelling growth of metal clusters on amorphous substrates, see Diczio & Wertheim (1989); the statistical mechanics of simple glass forming systems in 2D, see Hentschel et al. (2007); modelling of material interface evolution in grain growth of polycrystalline materials, see Lee & Chen (2006). When the seeds are randomly and uncorrelated distributed, are called Poisson Voronoi diagrams. A great number of natural phenomena are described by Poisson Voronoi diagrams, we cite some of them : lattices in quantum field theory, see Drouffe & Itzykson (1984); conductivity and percolation in granular composites, see Jerauld et al. (1984a) and Jerauld et al. (1984b); modelling growth of metal clusters on amorphous substrates, see Diczio & Wertheim (1989); the statistical mechanics of simple glass forming systems in 2D, see Hentschel et al. (2007); modelling of material interface evolution in grain growth of polycrystalline materials, see Lee & Chen (2006). A review of the Voronoi diagrams applied to the spatial distribution of the galaxies

can be found in Zaninetti (2006). Here we are interested in the fragmentation of a 2D layer of thickness negligible in respect to the main dimension. A typical dimension of the layer can be found as follows. The averaged observed diameter of the galaxies is

$$\overline{D^{obs}} \approx 0.6 D_{max}^{obs} = 2700 \frac{Km}{sec} = 27 \text{ Mpc} \quad , \quad (4)$$

where $D_{max}^{obs} = 4500 \frac{Km}{sec}$ corresponds to the extension of the maximum void visible on the CFA2 slices. In the framework of the theory of the primordial explosions, see Charlton & Schramm (1986) and Zaninetti & Ferraro (1990), this means that the mean observed area of a bubble, $\overline{A^{obs}}$, is

$$\overline{A^{obs}} \approx 4\pi \left(\frac{D_{max}^{obs}}{2} \right)^2 = 2290 \text{ Mpc}^2 \quad . \quad (5)$$

The averaged area of a face of Voronoi polyhedra, $\overline{A_V}$, is

$$\overline{A_V} = \frac{\overline{A^{obs}}}{\overline{N_F}} \quad , \quad (6)$$

where $\overline{N_F}$ is the averaged number of irregular faces of the Voronoi polyhedra, i.e. $\overline{N_F}=16$, see Okabe et al. (1992); Zaninetti (2006). The averaged side of a face of a irregular polyhedron, $\overline{L_V}$, is

$$\overline{L_V} \approx \sqrt{\overline{A^{obs}}} \approx 12 \text{ Mpc} \quad . \quad (7)$$

The thickness of the layer, δ , can be derived from the shock theory, see Bowers & Deeming (1984), and is 1/12 of the radius of the advancing shock,

$$\delta = \frac{D_{max}^{obs}}{2 \times 12} \approx 1.12 \text{ Mpc} \quad . \quad (8)$$

The number of galaxies in this typical layer, N_G , can be found by multiplying $n_* \approx 0.1$, the density of galaxies, for the volume of the cube of side 12 Mpc : i.e. $N_G \approx 172$.

The more common way to insert the seeds of the Voronoi polygons is a random sequence in the X and Y direction, see Figure 1.

The distribution of the area of the irregular Voronoi polygons is fitted with a Kiang function, see formula (A5) in Appendix A,:

$$H(x; c) = \frac{c}{\Gamma(c)} (cx)^{c-1} \exp(-cx) \quad , \quad (9)$$

and the captions of Figure 1 also report the value of c as deduced from the parameters of the sample.

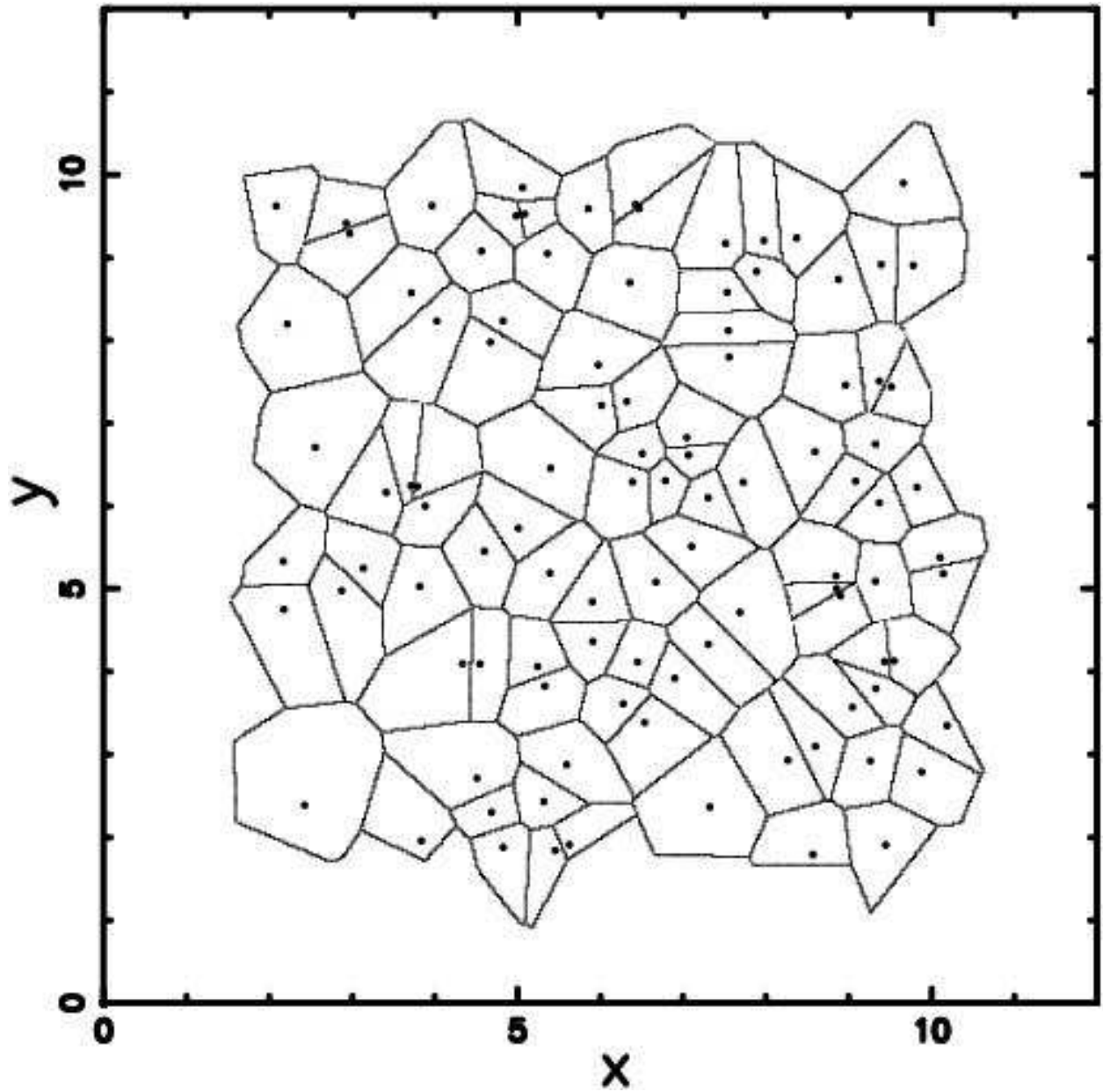


Fig. 1.— The Voronoi-diagram in 2D when random seeds are used. The selected region comprises 77 seeds and $c = 5.1$.

Another way to insert the seeds is through a truncated Pareto distribution , see Appendix B; this is an example of non-Poissonian seeds.

In polar coordinates the radial distribution of seeds $p(r)$ will vary according to

$$p(r) \propto \frac{1}{r^{d+1}} \quad , \quad (10)$$

where r is the distance from the center of the box , see Figure 2.

2.2. A first main physical luminosity distribution

In order to start, we briefly review how a probability density function (in the following pdf) $f(x)$ changes to $g(y)$ when a new variable $y(x)$ is introduced . We limit ourselves to the case in which $y(x)$ is a unique transformation. The rule for transforming a pdf is

$$g(y) = \frac{f(x)}{\left| \frac{dy}{dx} \right|} \quad . \quad (11)$$

We start by assuming that the masses of the galaxies are distributed like a Kiang function, see formula (A5) in Appendix A or the previous paragraph. This assumption is justified by the fact that the various processes that lead to the formation of a galaxy can follow a random fragmentation in 2D. The first transformation is

$$x = \frac{\mathcal{M}}{\mathcal{M}^*} \quad , \quad (12)$$

and therefore equation (A5) changes to

$$\Psi(\mathcal{M})d\mathcal{M} = \frac{\left(\frac{\mathcal{M}}{\mathcal{M}^*}\right)^{c-1} e^{-\frac{\mathcal{M}}{\mathcal{M}^*}}}{\Gamma(c)} d\frac{\mathcal{M}}{\mathcal{M}^*} \quad . \quad (13)$$

This is a gamma distribution with a scale parameter \mathcal{M}^* and a shape parameter c , and its averaged value is

$$\langle \mathcal{M} \rangle = c\mathcal{M}^* \quad . \quad (14)$$

The mass-luminosity relationship in the case of the stars is well established both from a theoretical point of view, $L \propto M^3$ or $L \propto M^4$,see Lang (1999), and from an observational point of view , $L \propto M^{3.43}$ in the case of MAIN,V , see Zaninetti (2005) for further details. A power law which is introduced by analogy regulates the relationship between mass and

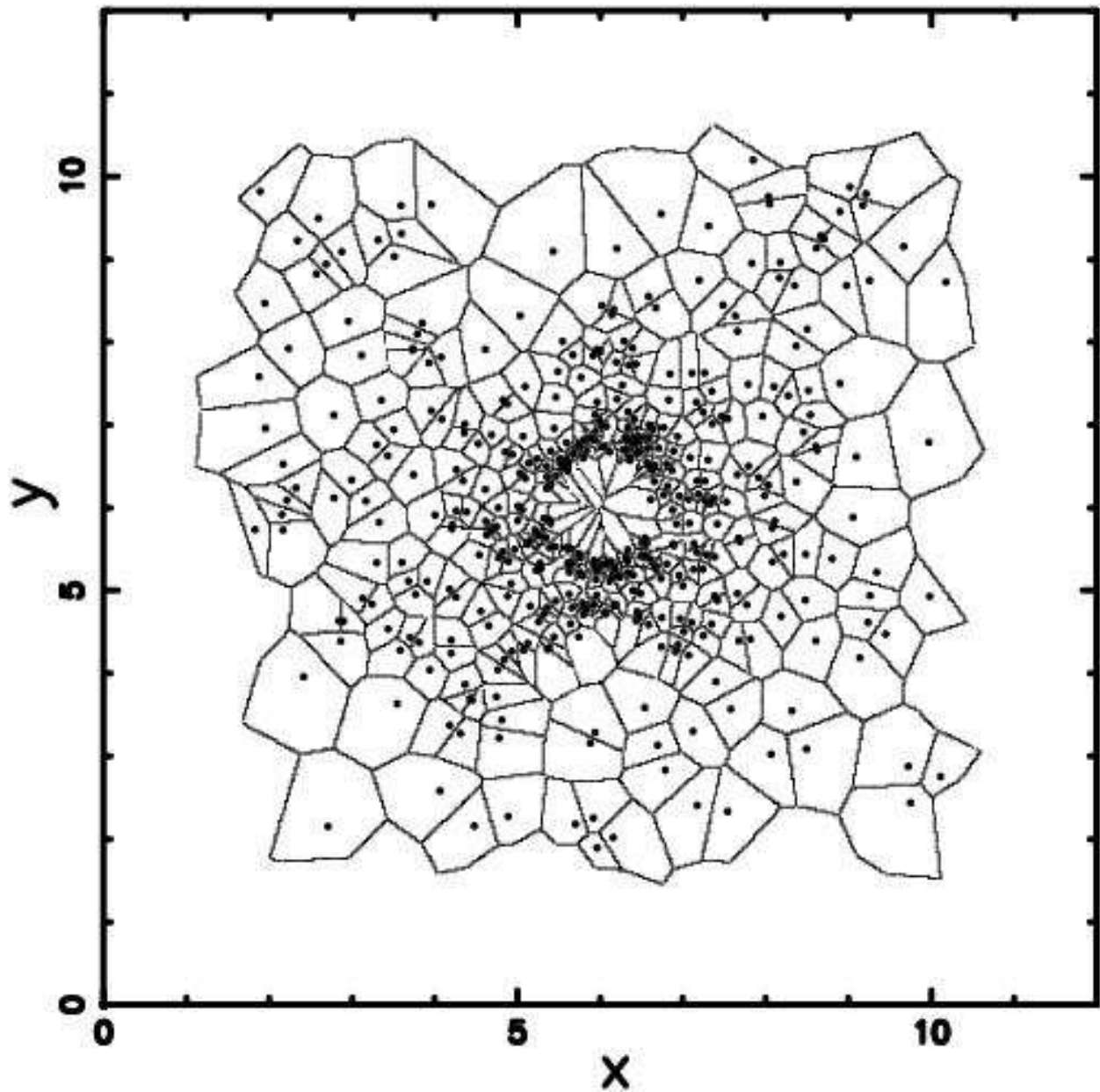


Fig. 2.— The Voronoi-diagram in 2D when truncated Pareto seeds are used. The selected region comprises 124 seeds and $d = 0.27$ as deduced from MLE , see Appendix B .

luminosity of galaxies, but in this case the regulating parameter a does not have a theoretical counterpart. The second transformation is

$$\frac{\mathcal{M}}{\mathcal{M}^*} = \left(\frac{L}{L^*} \right)^{\frac{1}{a}} , \quad (15)$$

where $1/a$ is an exponent that connects the mass to the luminosity. The pdf (13) is therefore transformed into the following:

$$\begin{aligned} \Psi(L)dL = & \left(\frac{1}{a\Gamma(c)} \right) \left(\frac{\Psi^*}{L^*} \right) \left(\frac{L}{L^*} \right)^{\frac{c-a}{a}} \\ & \times \exp \left(- \left(\frac{L}{L^*} \right)^{\frac{1}{a}} \right) dL , \end{aligned} \quad (16)$$

where Ψ^* is a normalisation factor which defines the overall density of galaxies, a number per cubic Mpc . The mathematical range of existence is $0 \leq L < \infty$; conversely the astronomical range is $L_{\min} \leq L < L_{\max}$.

The relationship connecting the absolute magnitude, M , of a galaxy with its luminosity is

$$\frac{L}{L_{\odot}} = 10^{0.4(M_{bol,\odot} - M)} , \quad (17)$$

where $M_{bol,\odot}$ is the bolometric luminosity of the sun, which according to Cox (2000) is $M_{bol,\odot} = 4.74$.

The third and last transformation connects the luminosity with the absolute magnitude

$$\begin{aligned} \Psi(M)dM = & \left(0.4 \ln 10 \frac{1}{a\Gamma(c)} \right) \Psi^* 10^{0.4(\frac{c}{a})(M^* - M)} \\ & \times \exp(-10^{0.4(M^* - M)(\frac{1}{a})}) dM . \end{aligned} \quad (18)$$

This data oriented function contains the parameters M^* , a , c and Ψ^* which can be derived from the operation of fitting the observational data. Other interesting quantities are the mean luminosity per unit volume, j ,

$$j = \int_0^{\infty} L \Psi(L) dL = L^* \Psi^* \frac{\Gamma(c+a)}{\Gamma(c)} , \quad (19)$$

and the averaged luminosity, $\langle L \rangle$,

$$\langle L \rangle = \frac{j}{\Psi^*} = L^* \frac{\Gamma(c+a)}{\Gamma(c)} . \quad (20)$$

The density of galaxies is

$$n_* = \frac{j}{L^*} \quad , \quad (21)$$

and the mean separation between galaxies ,

$$d_* = n_*^{-1/3} \quad . \quad (22)$$

The symbols j , n_* and d_* are introduced as in Padmanabhan (1996).

Another way to compute the density of galaxies , now n_{**} , of the $\mathcal{M} - L$ function is

$$n_{**} = \Psi^* \quad . \quad (23)$$

The position of the maximum in magnitudes is at

$$M_{p,max} = M^* - 1.085 \ln(c) a \quad . \quad (24)$$

2.3. The luminosity distribution for low luminosity galaxies

The Pareto distribution can model nonnegative data with a power law probability tail. In many practical applications, it is natural to consider an upper bound that truncates the tail Cohen & Whitten (1988); Devoto & Martnez (1998); Aban et al. (2006). The truncated Pareto distribution has a wide range of applications , we list some of them : data analysis Aban et al. (2006)and Rehfeldt et al. (1992); forest fire area in the Australian Capital Territory, fault offsets in the Vernejoul coal field, hydrocarbon volumes in the Frio Strand Plain exploration play and fault lengths on Venus, see Burroughs & Tebbens (2001).

In the case of the stars , the low mass distribution of masses , see Salpeter (1955), can be represented by a law of the type $p(\mathcal{M}_S) \propto \mathcal{M}_S^{-2.35}$, where $p(\mathcal{M}_S)$ represents the probability of having a mass between \mathcal{M}_S and $\mathcal{M}_S + d\mathcal{M}$. By analogy we introduce a truncated Pareto distribution, see Appendix B , for the mass of galaxies

$$\Psi_{LL}(\mathcal{M})d\mathcal{M} = \frac{C}{\left(\frac{\mathcal{M}}{\mathcal{M}^*}\right)^{d+1}} d\left(\frac{\mathcal{M}}{\mathcal{M}^*}\right) \quad , \quad (25)$$

where the index LL stands for Low Luminosity and the range of existence is $\mathcal{M}_{min} \leq \mathcal{M} \leq \mathcal{M}_{max}$ where min and max denote the minimum and maximum mass. Once the constant C is computed as in Appendix B we obtain

$$\Psi_{LL}(\mathcal{M})d\mathcal{M} = \frac{d}{\left(\left(\frac{\mathcal{M}_{min}}{\mathcal{M}^*}\right)^{-d} - \left(\frac{\mathcal{M}_{max}}{\mathcal{M}^*}\right)^{-d}\right) \left(\frac{\mathcal{M}}{\mathcal{M}^*}\right)^{d+1}} d\left(\frac{\mathcal{M}}{\mathcal{M}^*}\right) \quad . \quad (26)$$

Exactly as in the previous case we introduce the transformation represented by equation (15) that connects the mass with the luminosity and the distribution in luminosity is

$$\Psi_{LL}(L)dL = \Psi_{LL}^* \frac{d \left(\frac{L}{L^*} \right)^{-\frac{d+a}{a}}}{\left(\left(\frac{L_{min}}{L^*} \right)^{-\frac{d}{a}} - \left(\frac{L_{max}}{L^*} \right)^{-\frac{d}{a}} \right) a} d \left(\frac{L}{L^*} \right) , \quad (27)$$

with the range of existence as $L_{min} \leq L \leq L_{max}$ and Ψ_{LL}^* representing the normalisation. The mean luminosity per unit volume, j ,

$$j = \int_{L_{min}}^{L_{max}} L \Psi_{LL}(L) dL = \Psi_{LL}^* \frac{d \left(-L_{max}^2 \left(\frac{L_{max}}{L^*} \right)^{-\frac{d+a}{a}} + L_{min}^2 \left(\frac{L_{min}}{L^*} \right)^{-\frac{d+a}{a}} \right)}{(d-a) \left(\left(\frac{L_{min}}{L^*} \right)^{-\frac{d}{a}} - \left(\frac{L_{max}}{L^*} \right)^{-\frac{d}{a}} \right) L^*} . \quad (28)$$

The distribution in magnitude is

$$\Psi_{LL}(M)dM = \Psi_{LL}^* \frac{0.4 d 10^{-0.4 \frac{d(M^* - M)}{a}} \ln(10)}{\left(10^{-0.4 \frac{(M^* - M_{max})d}{a}} - 10^{-0.4 \frac{(M^* - M_{min})d}{a}} \right) a} dM , \quad (29)$$

with the range of existence as $M_{min} \leq M \leq M_{max}$. This distribution in magnitude contains the parameters M_{min} and M_{max} which are the minimum and maximum magnitude of the considered catalog and the parameters a , d , and Ψ_{LL} which are derived from the fitting of the data.

3. Application to a real sample of galaxies

The data of the luminosity function for galaxies in five bands of the SDSS are available at <http://cosmo.nyu.edu/blanton/lf.html> and are discussed from an astronomical point view in Blanton et al. (2001).

The analysis of the new luminosity function was split in two. The case from high luminosities to low luminosities was fitted by $\Psi(M)$, equation (18) . The data have been processed through the Levenberg–Marquardt method (subroutine MRQMIN in Press et al. (1992)) in order to find the three parameters a , M^* , Ψ^* ; c conversely is introduced by hand. In order to associate a statistical probability to each fit we have chosen a range in magnitude such as $M < M_{max}$ where M_{max} represents the selected maximum magnitude of the sample.

The results are reported in Table 2 together with the derived quantities j , n_* , d_* and their uncertainties. Table 2 also reports M_{max} , the number of elements N belonging to the

sample , the merit function χ^2 and the associated p -value that has to be understood as the maximum probability to obtain a better fitting, see formula (15.2.12) in Press et al. (1992):

$$p = 1 - GAMMQ(\frac{N-3}{2}, \frac{\chi^2}{2}) \quad , \quad (30)$$

where GAMMQ is a subroutine for the incomplete gamma function.

The uncertainties are found by implementing the error propagation equation (often called law of errors of Gauss). The low luminosities range conversely was fitted through $\Psi_{LL}(M)$, equation (29) and the results are reported in Table 3.

Table 2. Parameters of Fits to Luminosity Function in SDSS Galaxies through the $\mathcal{M} - L$ function .

Band	u^*	g^*	r^*	i^*	z^*
c	1.1 ± 0.2	1.0 ± 0.2	1.1 ± 0.2	2 ± 0.2	1.7 ± 0.2
M^* [mags]	-16.58 ± 0.018	-18.29 ± 0.008	-18.77 ± 0.007	-18.26 ± 0.01	-18.79 ± 0.004
Ψ^* [$h \text{ Mpc}^{-3}$]	0.069 ± 0.001	0.043 ± 0.0003	0.043 ± 0.000	0.032 ± 0.0002	0.034 ± 0.003
a	1.40 ± 0.007	1.32 ± 0.003	1.5 ± 0.002	1.74 ± 0.003	1.70 ± 0.014
j [mags]	$1.40 L^* \Psi^*$	$1.18 L^* \Psi^*$	$1.50 L^* \Psi^*$	$4.39 L^* \Psi^*$	$3.2 L^* \Psi^*$
n_* [Mpc^{-3}]	0.097 ± 0.022	0.051 ± 0.012	0.066 ± 0.016	0.14 ± 0.02	0.11 ± 0.04
d [Mpc]	2.17 ± 0.16	2.67 ± 0.21	2.47 ± 0.19	1.91 ± 0.09	2.06 ± 0.14
M_{max} [mags]	-15.78	-18.2	-19	-19.3	-20
N	483	404	400	471	442
χ^2	321	386	233	325	649
$p = 1 - \text{GAMMQ}(\frac{N-3}{2}, \frac{\chi^2}{2})$	0	0.31	0	$1.19 \cdot 10^{-7}$	1.0

The Schechter function, conversely fits all the range in luminosities and Table 4 reports the data that come out from the fitting procedure. Table 4 also reports $M_{p,max}$, the value in magnitude where the Schechter function peaks ; this value is defined when $\alpha = 1$, otherwise we leave the box blank.

Table 3. Parameters of Fits to Luminosity Function in SDSS Low Luminosities Galaxies through the Ψ_{LL} function .

Band	g^*	r^*	i^*	z^*
d	0.3 ± 0.1	0.4 ± 0.1	0.5 ± 0.1	0.9 ± 0.1
$M^* [mags]$	-17.2 ± 0.1	-18.8 ± 0.1	-17.39 ± 0.1	-19.3 ± 0.1
$\Psi_{LL}^* [h \text{ Mpc}^{-3}]$	0.043 ± 0.0043	0.040 ± 0.0040	0.026 ± 0.0032	0.035 ± 0.003
a	2.2 ± 0.1	1.3 ± 0.1	2.7 ± 0.1	2.3 ± 0.1
range [mags]	$-18.2 \leq M \leq 16.33$	$-19.0 \leq M \leq 16.31$	$-19.3 \leq M \leq 17.22$	$-20.0 \leq M \leq 17.48$
N	194	273	237	297
χ^2	204	379	476	313

Table 5 reports the χ^2 of the two zones of the new physical function, their sum and χ^2 of the Schechter luminosity function.

Table 4. Parameters of Fits to Luminosity Function in SDSS through the Schechter function .

Band	u^*	g^*	r^*	i^*	z^*
α	-0.90 ± 0.01	-0.88 ± 0.007	-1.04 ± 0.004	-0.99 ± 0.005	-1.07 ± 0.02
$M^* [mags]$	-17.92 ± 0.006	-19.38 ± 0.004	-20.43 ± 0.003	-20.81 ± 0.004	-21.18 ± 0.017
$M_{p,max} [mags]$	-17.92	-19.38		-20.81	
$\Phi^* [h \text{ Mpc}^{-3}]$	0.030 ± 0.0003	0.021 ± 0.0001	0.015 ± 0.00008	0.0147 ± 0.00008	0.0135 ± 0.00006
j [mags]	$0.95 L^* \Phi^*$	$0.92 L^* \Phi^*$	$1.02 L^* \Phi^*$	$0.99 L^* \Phi^*$	$1.04 L^* \Phi^*$
$n_* [Mpc^{-3}]$	0.029 ± 0.0003	0.02 ± 0.0001	0.015 ± 0.00007	0.014 ± 0.00008	0.014 ± 0.00007
d [Mpc]	3.24 ± 0.013	3.64 ± 0.006	4.02 ± 0.006	4.08 ± 0.008	4.12 ± 0.007
N	483	599	674	709	740
χ^2	330	753	2260	2282	3245
$p = 1 - GAMMQ(\frac{N-3}{2}, \frac{\chi^2}{2})$	$5.96 \cdot 10^{-8}$	0.99	1.0	1.0	1.0

The Schechter function , the new function and the data are reported in Figure 3 , Figure 4 , Figure 5 , Figure 6 , and Figure 7 when the u^*, g^*, r^*, i^* and z^* bands are considered; Figure 8 , Figure 9 , Figure 10 , Figure 11 , and Figure 12 report the residuals of the u^*, g^*, r^*, i^* and z^* band. We have used $H_0 = 100h \text{ km s}^{-1} \text{ Mpc}^{-1}$, with $h = 1$ in all the numerical evaluations. Due to the testing phase of the new $\mathcal{M} - L$ function, we have omitted the propagation of other values of h on the derived quantities , see the discussion in Blanton et al. (2001).

Table 5. Synoptic χ^2 .

Band		u^*	g^*	r^*	i^*	z^*
χ^2	physical luminosity function	321	386	233	325	649
χ^2	luminosity function low luminosities	0	204	379	476	313
	χ^2 sum of two zones	321	590	612	801	962
χ^2	Schechter luminosity function	330	753	2260	2282	3245

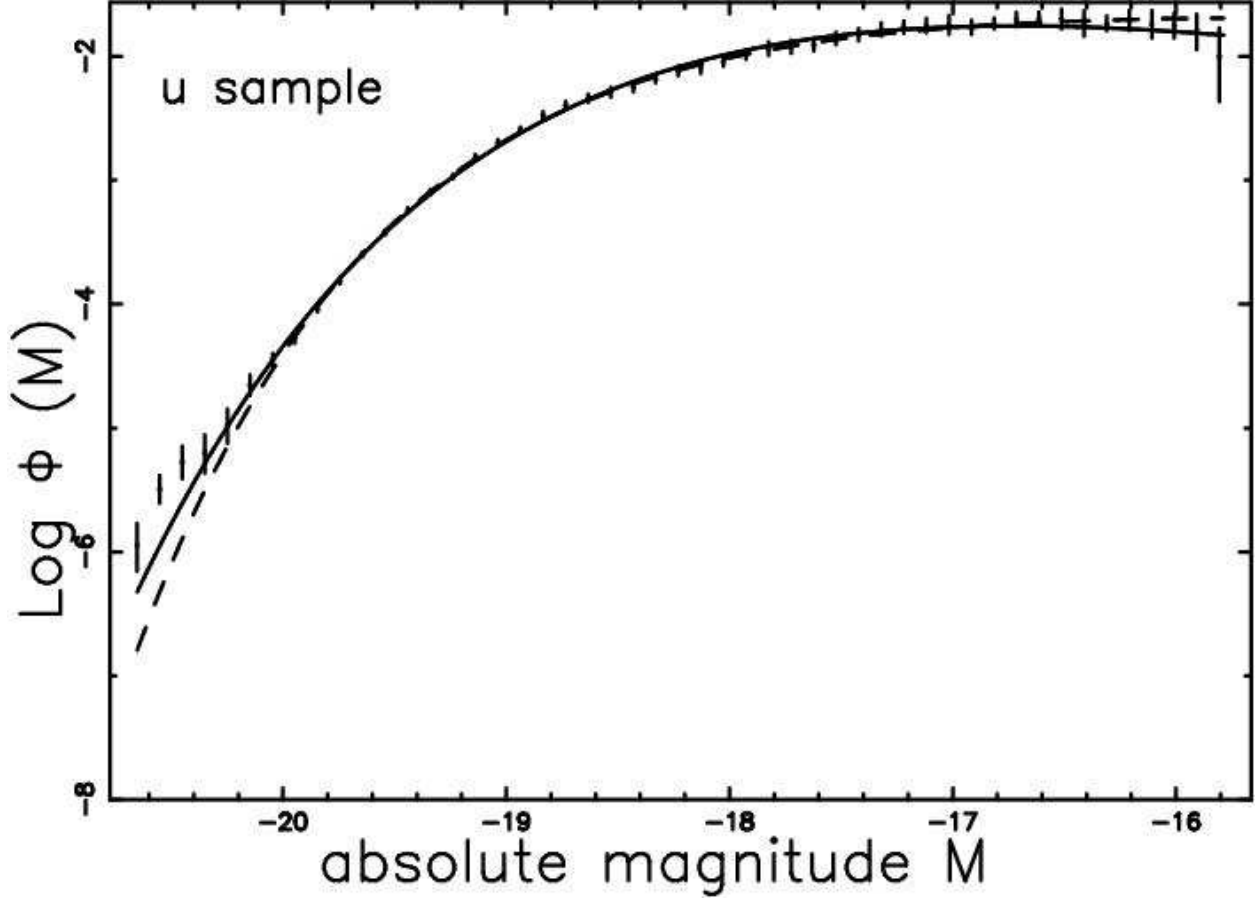


Fig. 3.— The luminosity function data of SDSS(u^*) are represented through the error bar. The fitting continuous line represents our two luminosity functions ((18) and (29)) and the dotted line represents the Schechter function.

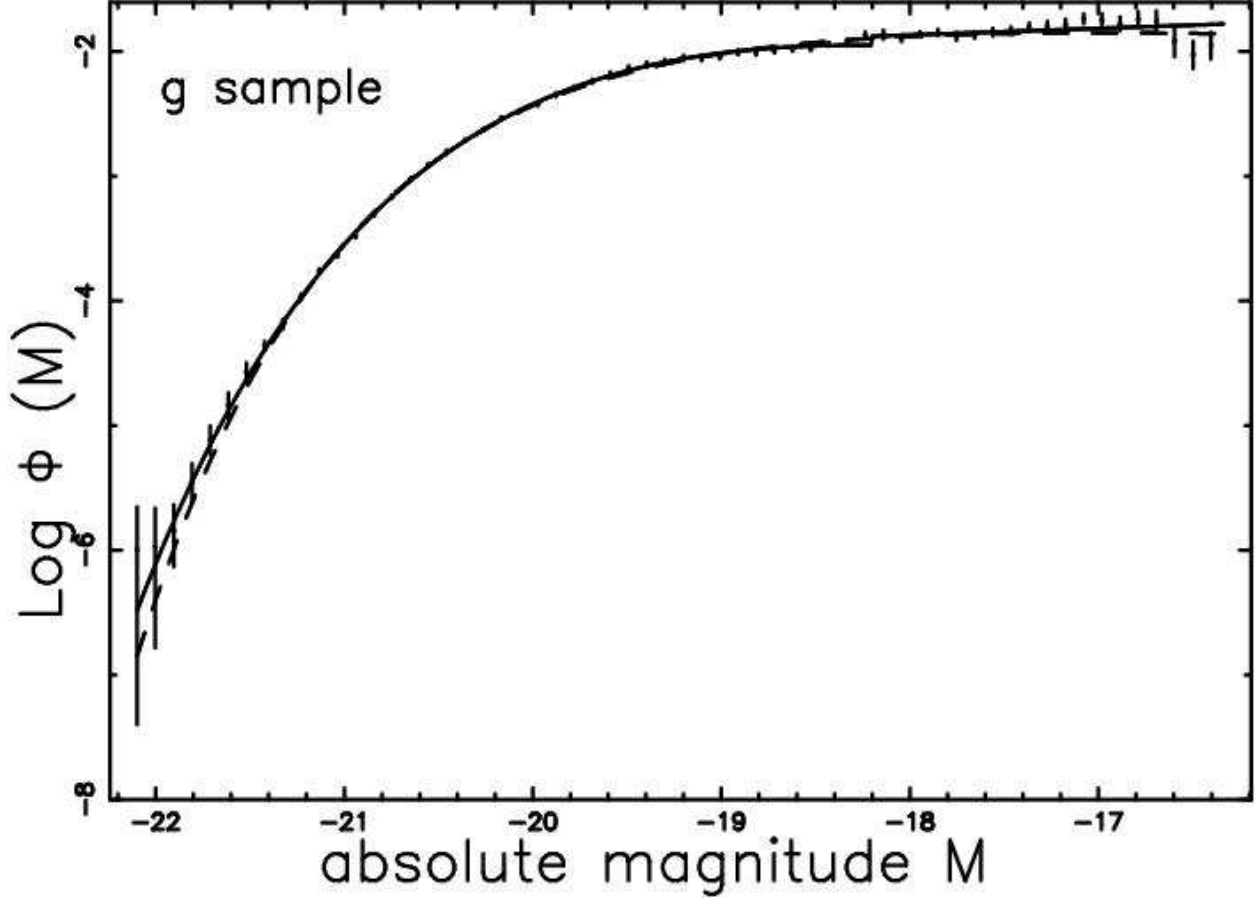


Fig. 4.— The luminosity function data of SDSS(g^*) are represented through the error bar. The fitting continuous line represents our two luminosity functions ((18) and (29)) and the dotted line represents the Schechter function.

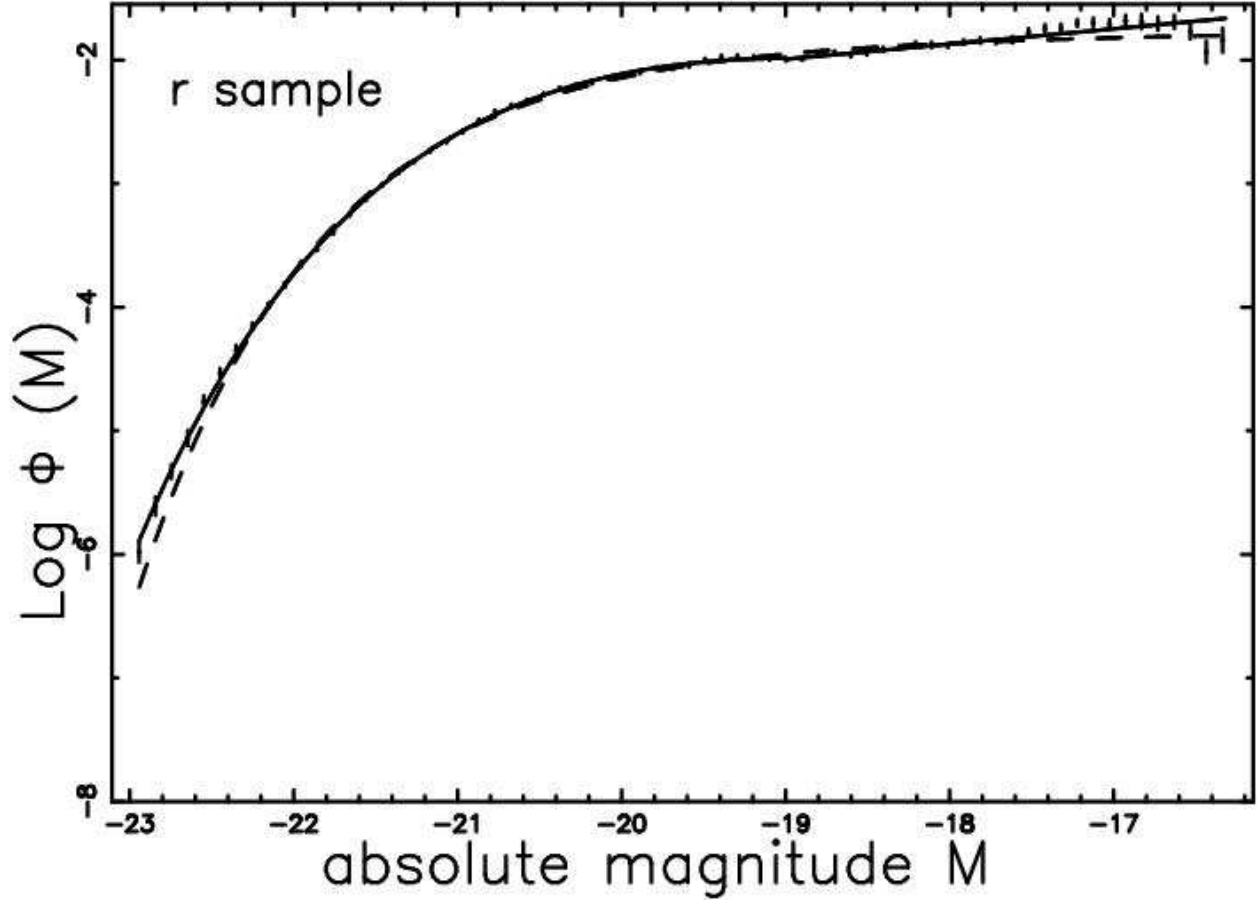


Fig. 5.— The luminosity function data of SDSS(r^*) are represented through the error bar. The fitting continuous line represents our two luminosity functions ((18) and (29)) and the dotted line represents the Schechter function.

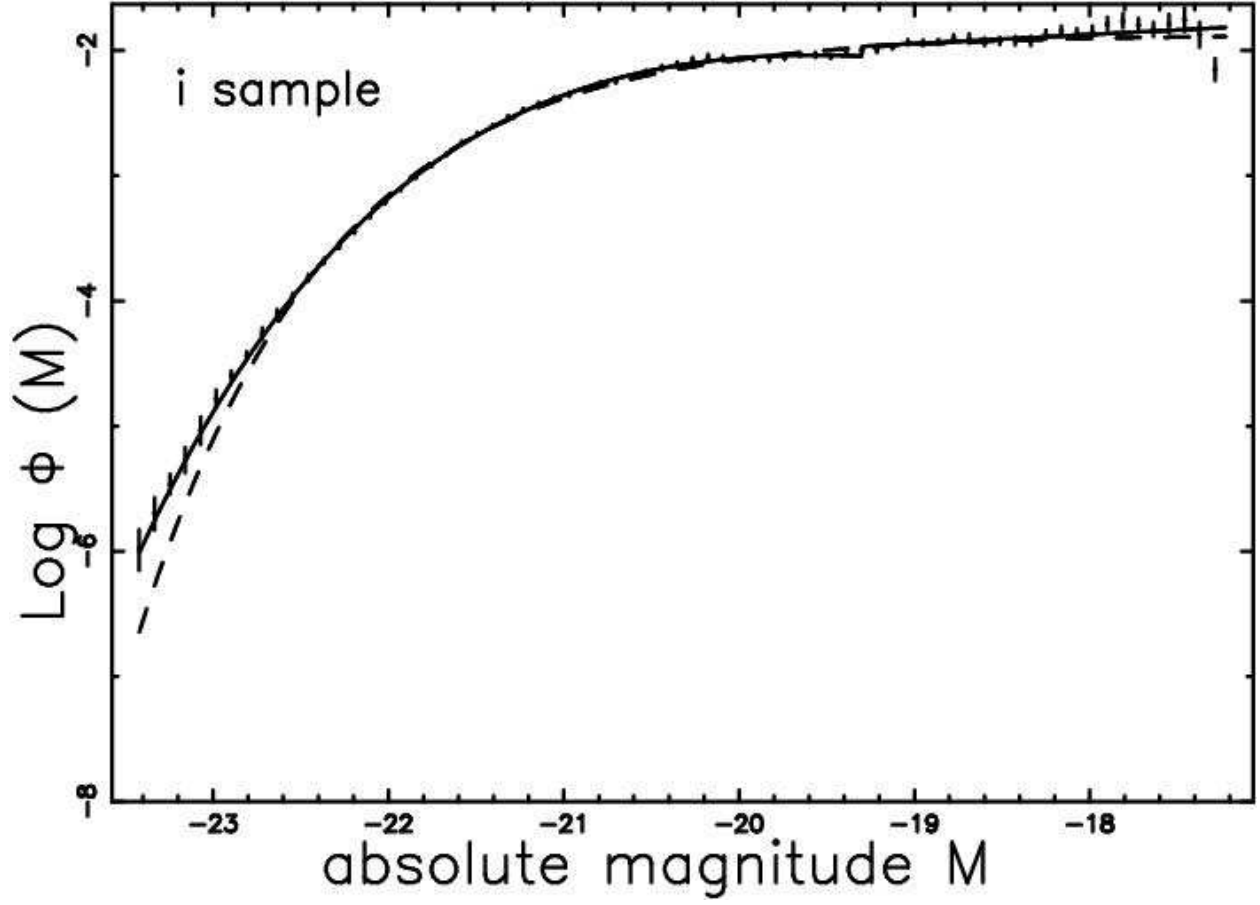


Fig. 6.— The luminosity function data of SDSS(i^*) are represented through the error bar. The fitting continuous line represents our two luminosity functions ((18) and (29)) and the dotted line represents the Schechter function.

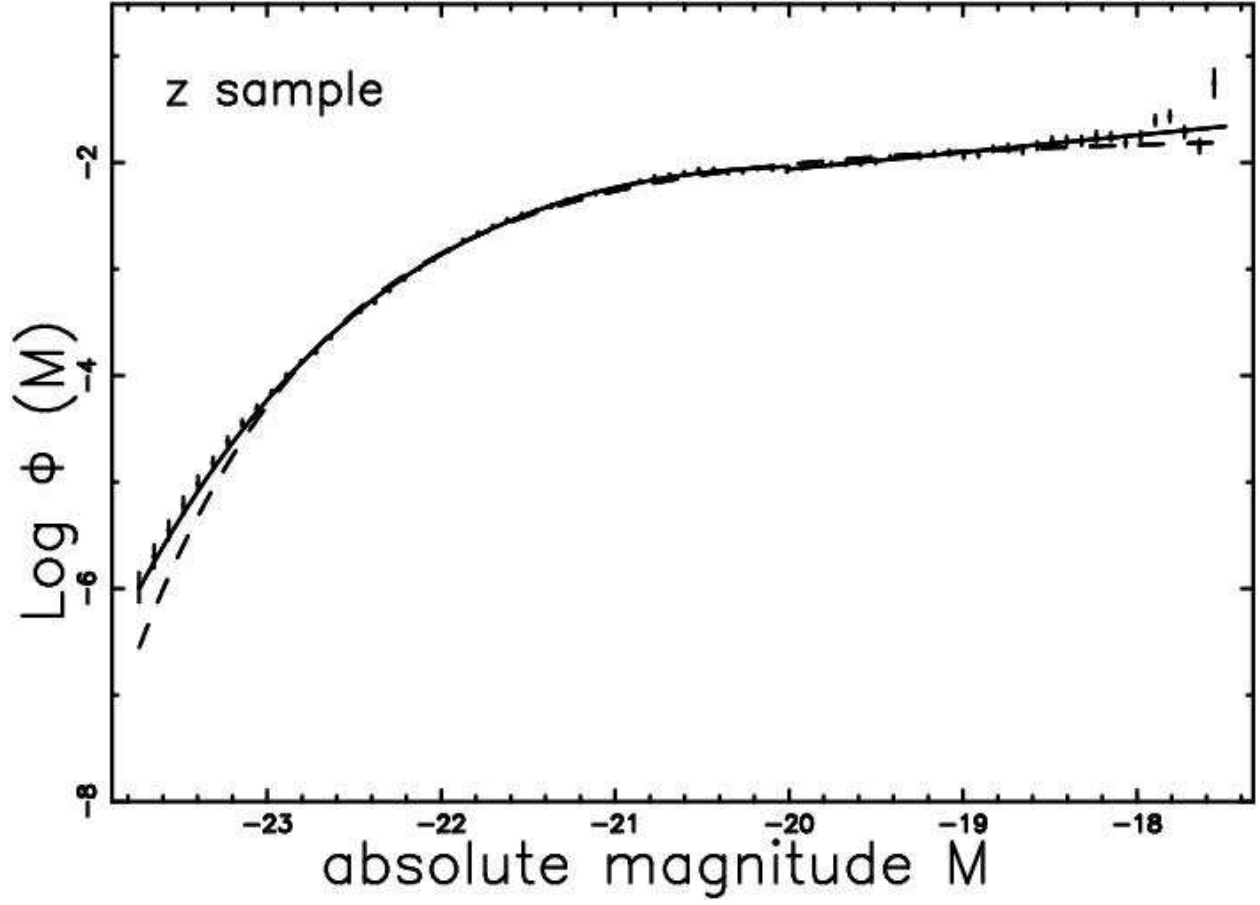


Fig. 7.— The luminosity function data of SDSS(z^*) are represented through the error bar. The fitting continuous line represents our two luminosity functions ((18) and (29)) and the dotted line represents the Schechter function.

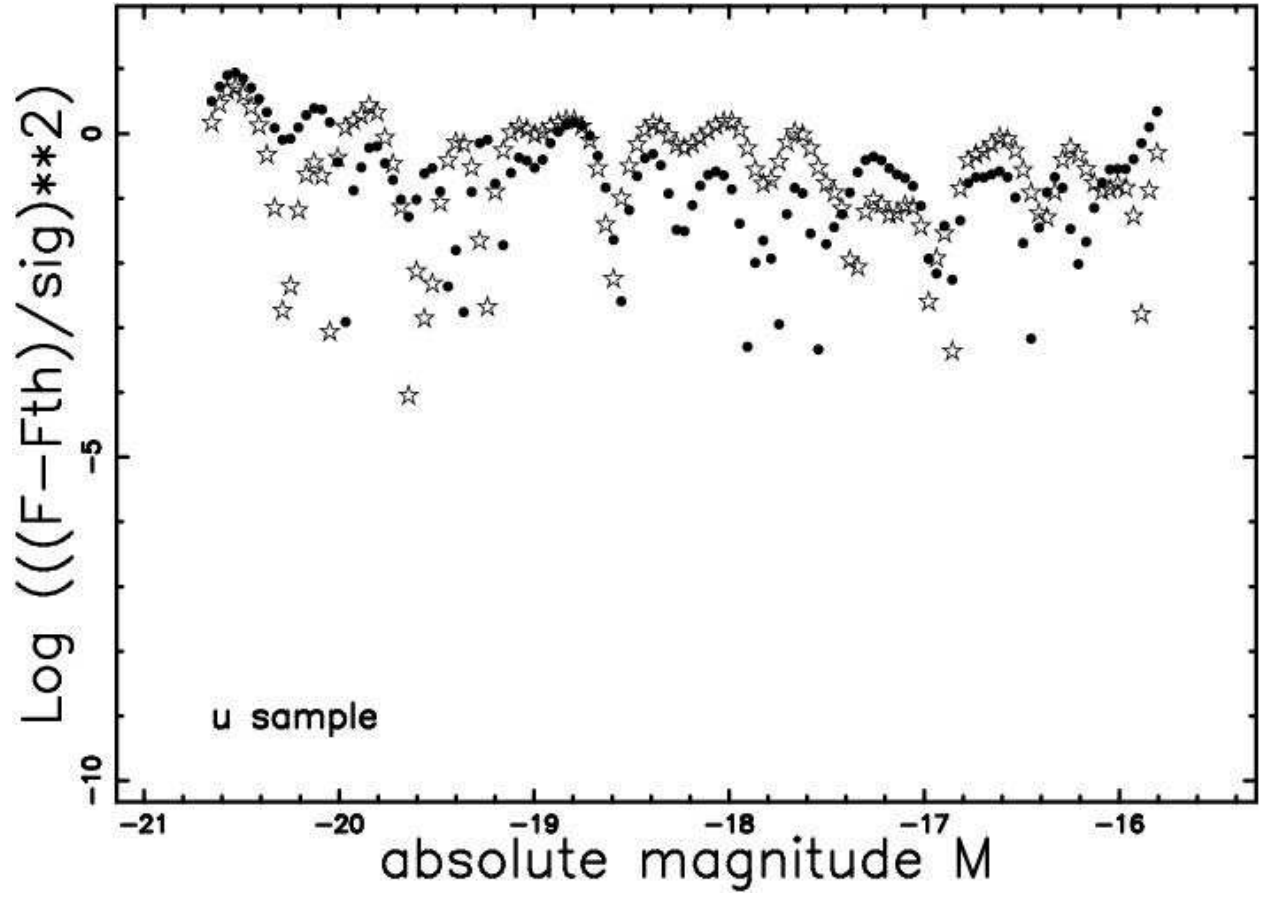


Fig. 8.— The residuals of the fits to SDSS(u^*) data. The empty stars represent our two luminosity functions ((18) and (29)) and the filled points represent the Schechter function.

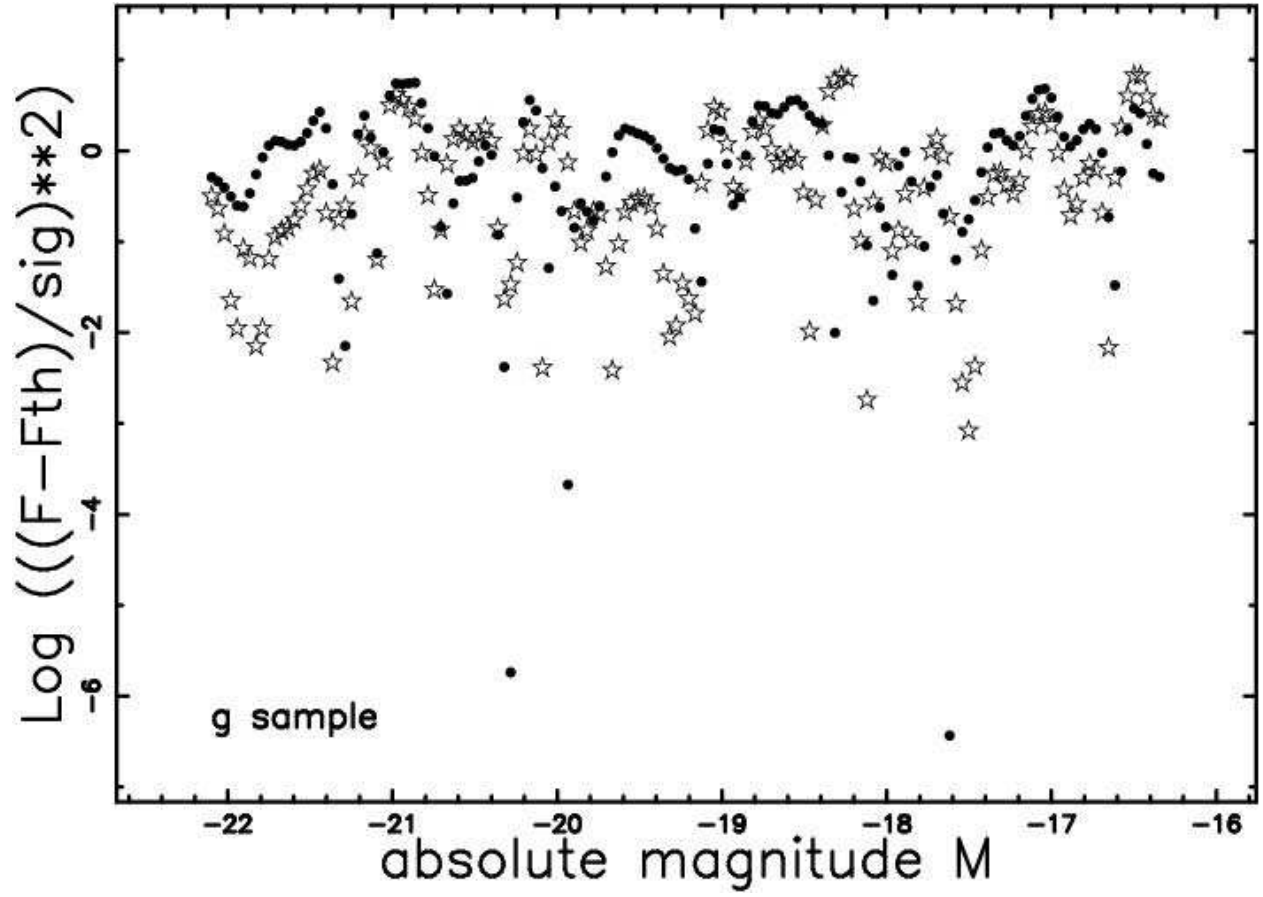


Fig. 9.— The residuals of the fits to SDSS(g^*) data. The empty stars represent our two luminosity functions ((18) and (29)) and the filled points represent the Schechter function.

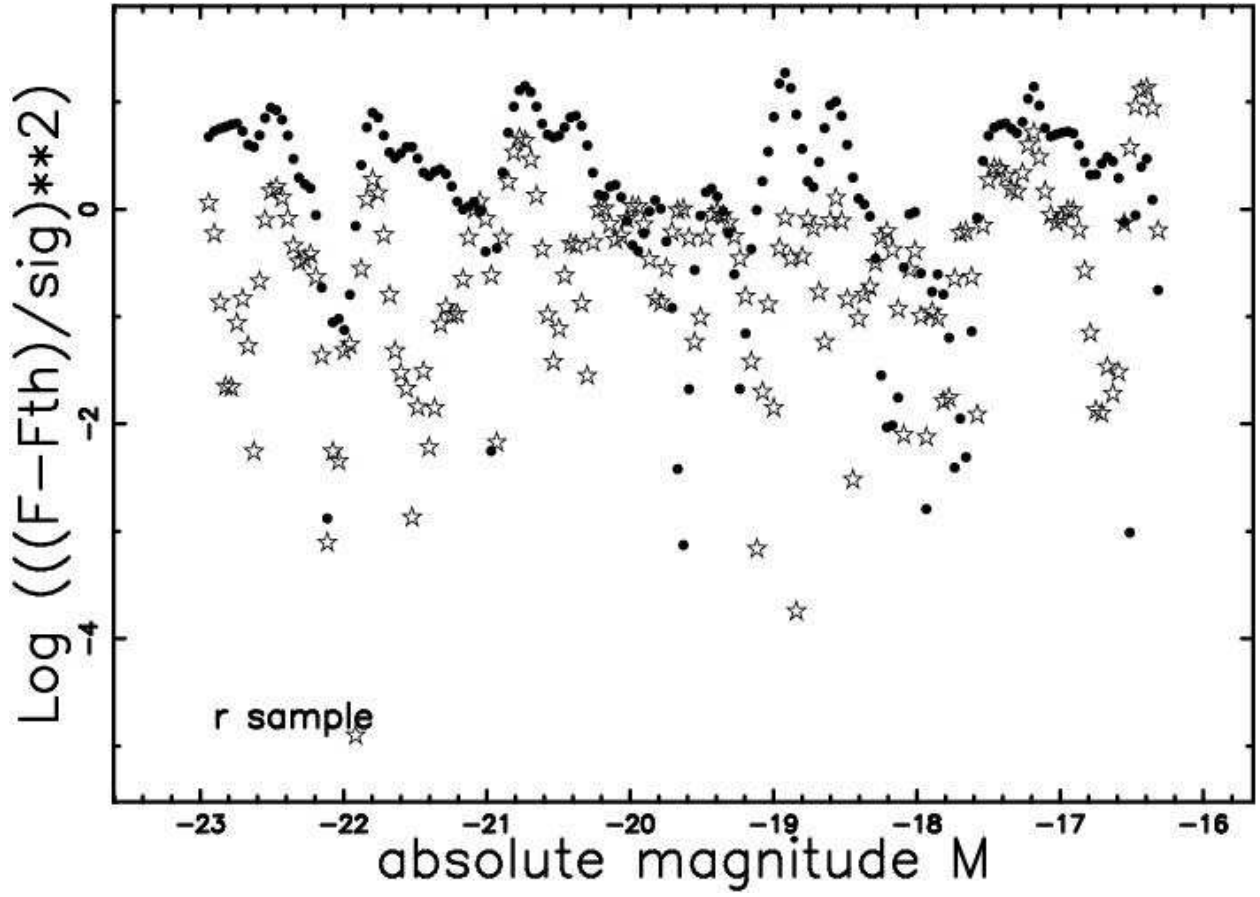


Fig. 10.— The residuals of the fits to SDSS(r^*) data. The empty stars represent our two luminosity functions ((18) and (29)) and the filled points represent the Schechter function.

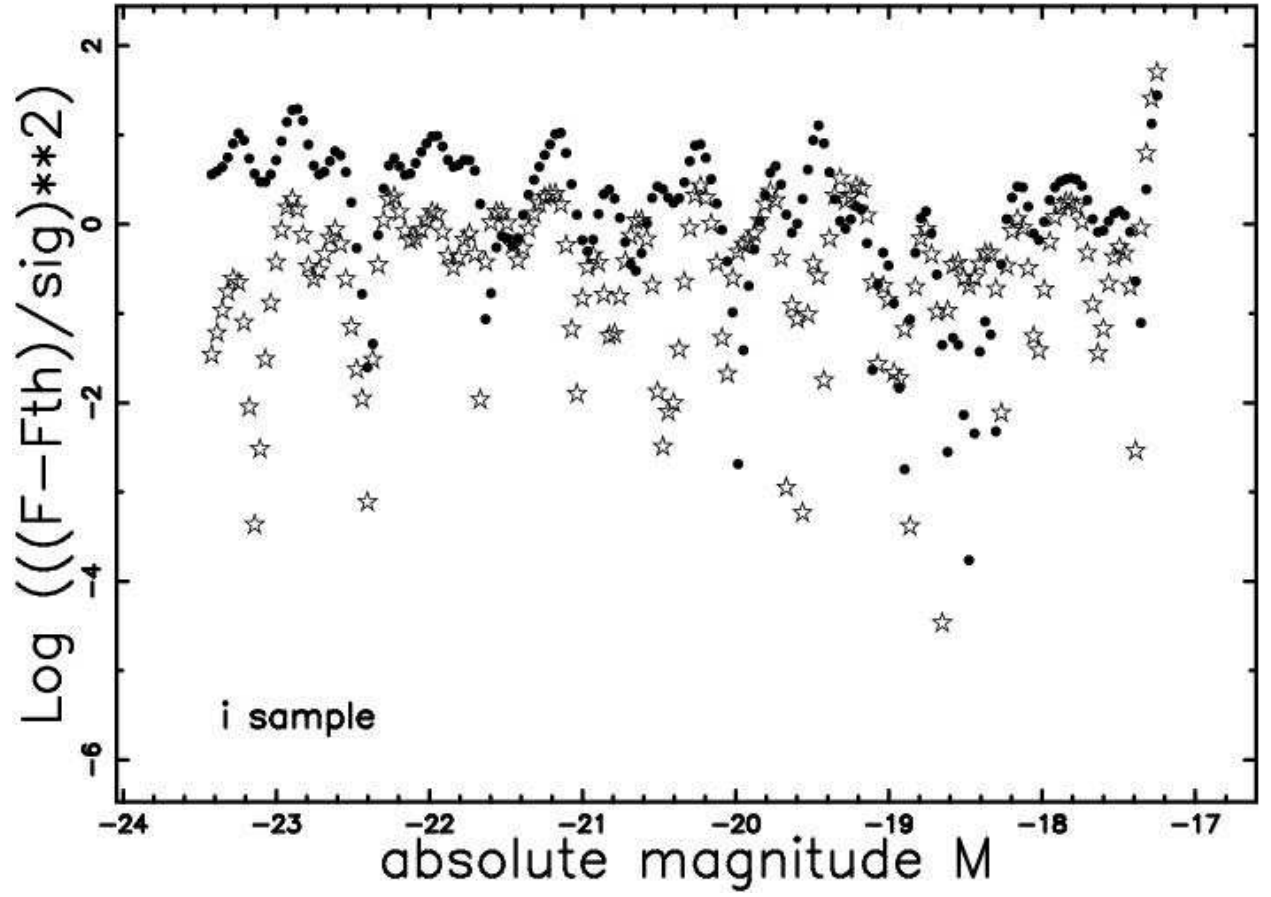


Fig. 11.— The residuals of the fits to SDSS(i^*) data. The empty stars represent our two luminosity functions ((18) and (29)) and the filled points represent the Schechter function.

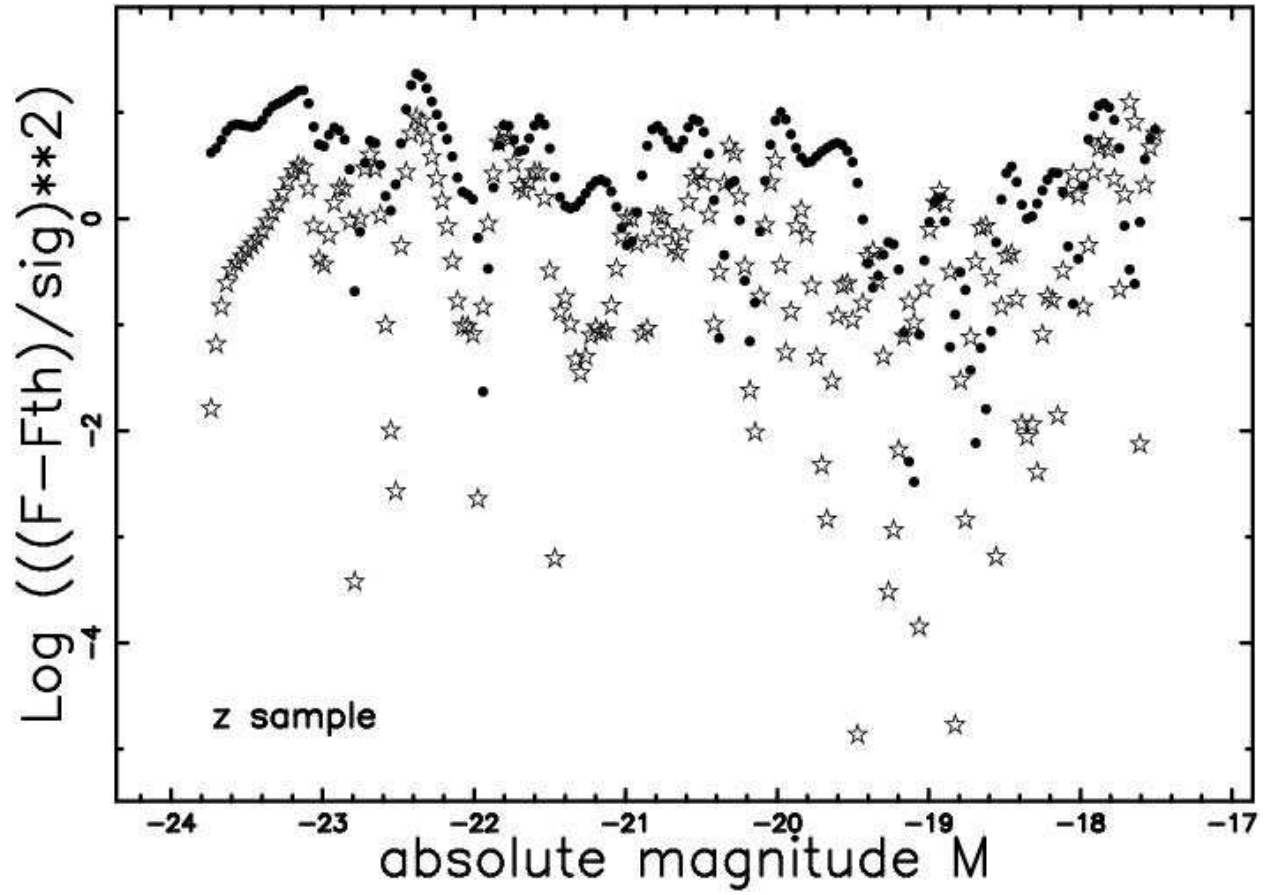


Fig. 12.— The residuals of the fits to SDSS(z^*) data. The empty stars represent our two luminosity functions ((18) and (29)) and the filled points represent the Schechter function.

The value obtained for the parameter a should be compared with that of the normal stars which is 3 or 4 as suggested by the theory, see for example Lang (1999), or ≈ 3.8 as suggested by the observations for $\mathcal{M} > 0.2\mathcal{M}_\odot$, see for example Cox (2000). When the three classes of stars are considered we have $a=3.43$ (MAIN), $a=2.79$ (GIANTS) and $a=2.43$ (SUPERGIANTS), see Zaninetti (2005) for further details.

The variation of j when the range in magnitude is finite rather than infinite can be evaluated by coupling together formula (17) and (18)

$$j = \int_{-21}^{-15.78} 10^{0.4(M_{bol,\odot}-M)} \Psi(M) dM \quad . \quad (31)$$

On inserting the parameters of SDSS band u^* (which is the case in which the $\mathcal{M} - L$ function covers all the range in magnitude of the data , see Table 2) and $M_{bol,\odot}=M_{u^*\odot}=6.39$, $j = 1.4 \cdot 10^8 L_\odot$ is obtained. This value increases by 5.63 % when the range is infinite; see a similar discussion concerning Schechter's function around formula (33) in Lin et al. (1996).

In absence of observational data that represent the luminosity function, we can generate them through Schechter's parameters, see Table 1. This is done, for example for the 2dF Galaxy Redshift Survey (2dFGRS) ,see Cross et al. (2001) and data of the Schechter function in Table 1. The parameters of the $\mathcal{M} - L$ function are reported in Table 6 where the requested errors on the values of luminosity are the same as the considered value.

4. Tests involving z

Some useful formulae connected with the Schechter function in a Euclidean ,non-relativistic and homogeneous universe are reviewed ; by analogy new formulae for the first part of the $\mathcal{M} - L$ function are derived.

Table 6: The parameters of the $\mathcal{M} - L$ luminosity function based on 2dFGRS data (triplets generated by the author)

<i>2dFGRS</i>	
c	0.1
$M^*[mags]$	-19 ± 0.1
$\Psi^*[h \text{ Mpc}^{-3}]$	0.4 ± 0.01
a	1.3 ± 0.1

4.1. The behaviour of the Schechter function

The flux of radiation , f , is introduced

$$f = \frac{L}{4\pi r^2} \quad , \quad (32)$$

where r represents the distance of the galaxy . The joint distribution in z and f for galaxies , see formula (1.104) in Padmanabhan (1996) , is

$$\frac{dN}{d\Omega dz df} = 4\pi \left(\frac{c}{H_0}\right)^5 z^4 \Phi\left(\frac{z^2}{z_{crit}^2}\right) \quad , \quad (33)$$

where $d\Omega$, dz and df represent the differential of the solid angle , the red-shift and the flux respectively. The L^* of difference between the previous formula and formula (1.104) in Padmanabhan (1996) is due to the small difference in the definition of Φ .

The formula for z_{crit} is

$$z_{crit}^2 = \frac{H_0^2 L^*}{4\pi f c_L^2} \quad , \quad (34)$$

where c_L represents the light velocity; the CODATA recommends $c_L = 299792.458 \frac{km}{s}$. The mean red-shift of galaxies with a flux f , see formula (1.105) in Padmanabhan (1996) , is

$$\langle z \rangle = z_{crit} \frac{\Gamma(3 + \alpha)}{\Gamma(5/2 + \alpha)} \quad . \quad (35)$$

The number density of galaxies per unit flux interval, see formula (1.106) in Padmanabhan (1996) , is

$$\frac{dN}{d\ln f} = \frac{\Phi^*}{2} \left(\frac{L^*}{4\pi f}\right)^{3/2} \Gamma\left(\frac{5}{2} + \alpha\right) \quad . \quad (36)$$

The number of galaxies in z and f as given by formula (33) has a maximum at $z = z_{max}$, where

$$z_{max} = z_{crit} \sqrt{\alpha + 2} \quad . \quad (37)$$

The value of z_{max} can be derived from the histogram of the observed number of galaxies expressed as a function of z . For practical purposes we analysed the 2dFGRS data release available at the web site: <http://msowww.anu.edu.au/2dFGRS/>. In particular we added together the file parent.ngp.txt that contains 145652 entries for NGP strip sources and the file parent.sgp.txt that contains 204490 entries for SGP strip sources. Once the heliocentric red-shift was selected we processed 219107 galaxies with $0.001 \leq z \leq 0.25$. A comparison between the observed and theoretical number of galaxies as a function of z is reported in Figure 13.

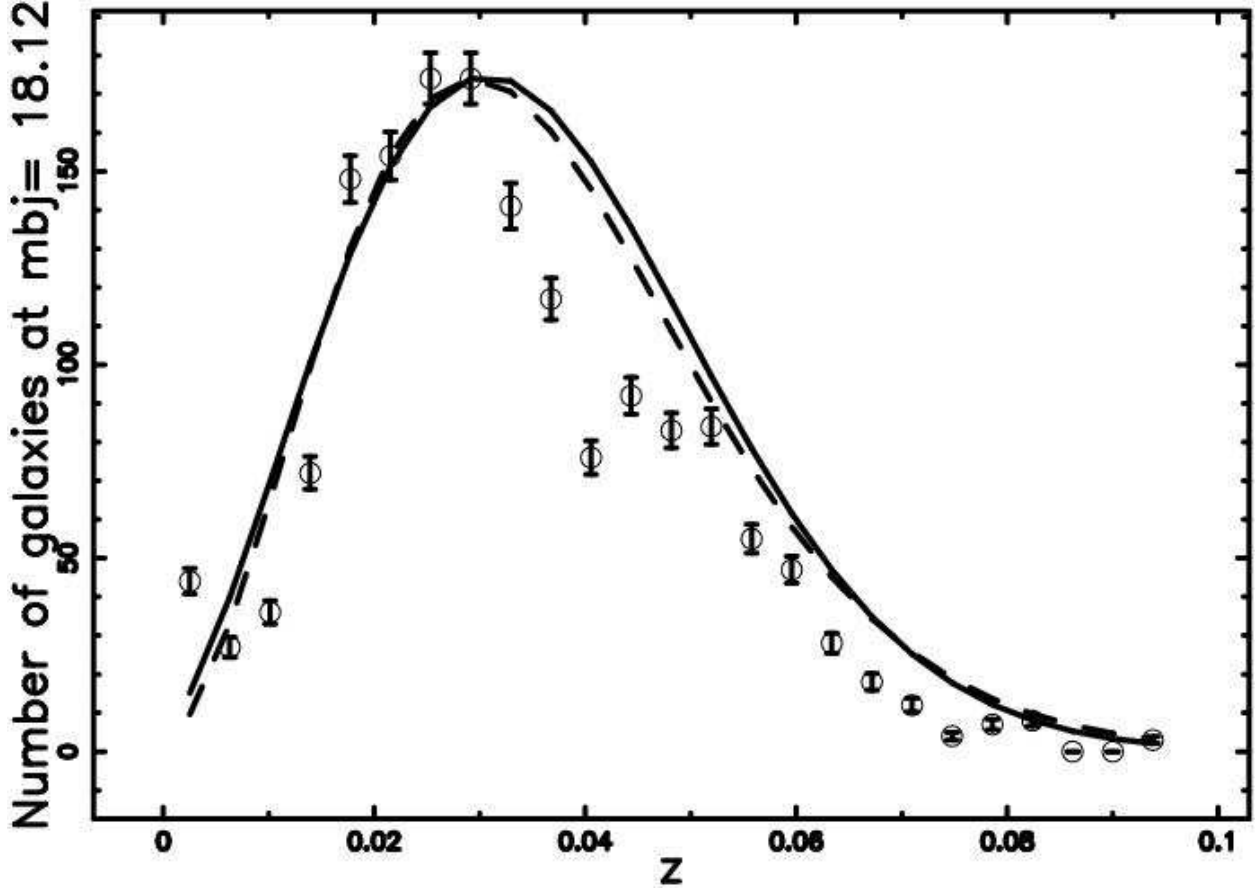


Fig. 13.— The galaxies of the 2dF Galaxy Redshift Survey with $15.08 \leq bJmag \leq 15.81$ (with $bJmag$ representing the relative magnitude used in object selection), are isolated in order to represent a chosen value of f and then organised in frequencies versus heliocentric redshift , (empty circles); the error bar is given by the square root of the frequency. The theoretical curve generated by the Schechter function of luminosity (formula (33) and parameters as in column 2dFGRS of Table 1) is drawn (full line). The theoretical curve generated by the $\mathcal{M} - L$ function for luminosity (formula (38) and parameters as in column 2dFGRS of Table 6) is drawn (dashed line); $\chi^2 = 320$ for the Schechter function and $\chi^2 = 283$ for the $\mathcal{M} - L$ function.

Another interesting catalog is the 6dF Galaxy Survey that has measured around 150000 redshifts and 15000 peculiar velocities from galaxies over the southern sky , see Jones et al. (2006). It is available at the following address <http://vizier.u-strasbg.fr/viz-bin/VizieR?-source=VII/249> ; we selected the re-calibrated bJ magnitude and the recession velocity cz . Figure 14 reports the observed and theoretical number of galaxies as a function of z for the 6dF Galaxy Survey.

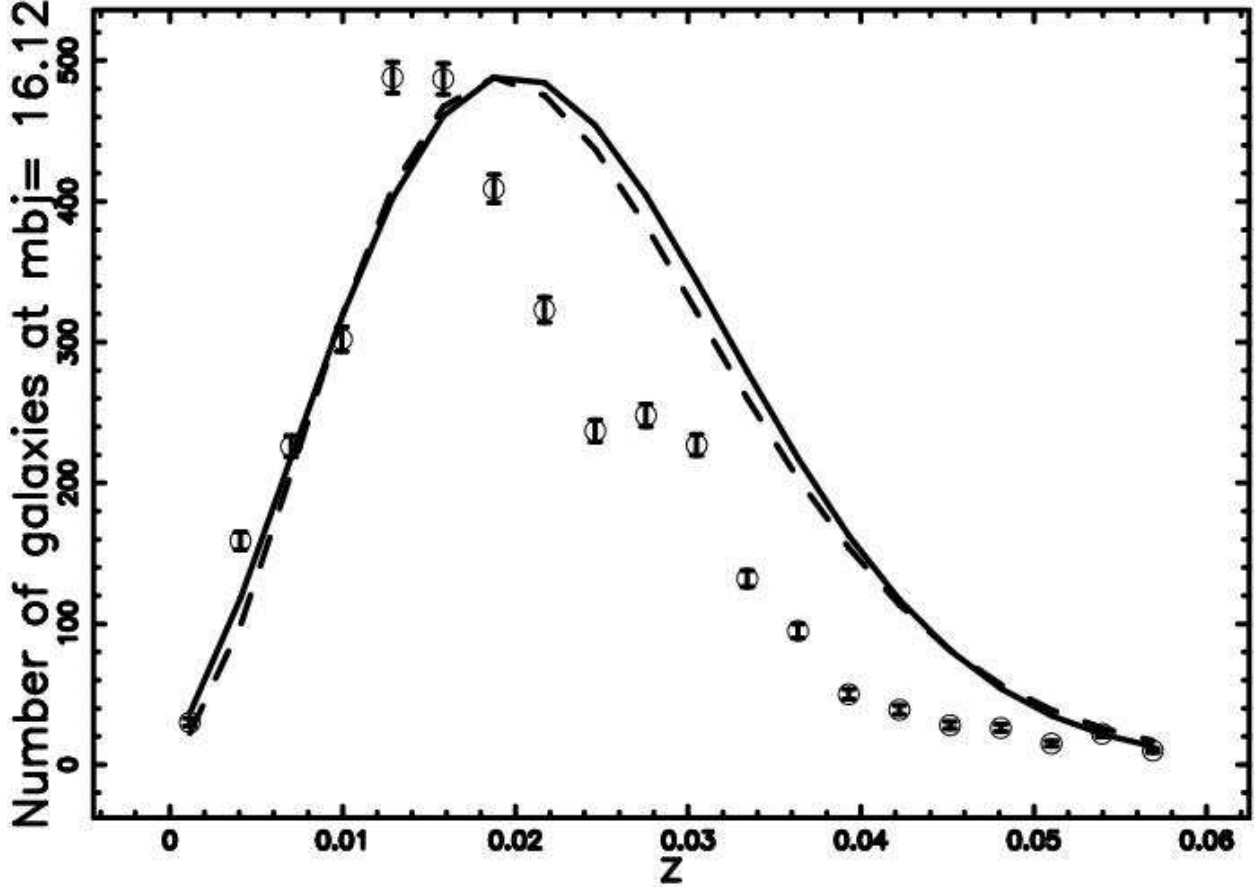


Fig. 14.— The galaxies of the 6dF Galaxy Survey with $14.15 \leq bJmag \leq 14.9$ (with $bJmag$ representing the relative magnitude used in object selection), are isolated in order to represent a chosen value of f and then organised in frequencies versus redshift , (empty circles); the error bar is given by the square root of the frequency. The theoretical curve generated by the Schechter function of luminosity (formula (33) and parameters as in column 2dFGRS of Table 1) is drawn (full line). The theoretical curve generated by the $\mathcal{M} - L$ function for luminosity (formula (38) and parameters in column 2dFGRS of Table 6) is drawn (dashed line); $\chi^2= 1373$ for the Schechter function and $\chi^2= 1197$ for the $\mathcal{M} - L$ function.

4.2. The behaviour of the $\mathcal{M} - L$ function

The joint distribution in z and f , in presence of the $\mathcal{M} - L$ luminosity (equation (16)) is

$$\frac{dN}{d\Omega dz df} = 4\pi \left(\frac{c}{H_0}\right)^5 z^4 \Psi\left(\frac{z^2}{z_{crit}^2}\right) . \quad (38)$$

The mean red-shift is

$$\langle z \rangle = z_{crit} \frac{2 \cdot 4^{-\frac{2a+c}{a}} \Gamma(2a+c) 2^{\frac{2c+3a}{a}}}{\Gamma(c+3/2a)} . \quad (39)$$

The number density of galaxies per unit flux interval is

$$\frac{dN}{d\ln f} = \frac{1}{16} \frac{L_*^{3/2} \Psi_* \Gamma(c + \frac{3}{2}a)}{\pi^{3/2} f^{3/2} \Gamma(c)} . \quad (40)$$

The number of galaxies as given by formula (38) has a maximum at z_{max} where

$$z_{max} = z_{crit} (c+a)^{a/2} . \quad (41)$$

A comparison between the observed and theoretical number of galaxies as given by the $\mathcal{M} - L$ function is reported in Figure 13 where the 2dF Galaxy Redshift Survey is considered and in Figure 14 where the 6dF Galaxy Survey is considered.

5. Mass evaluation

One method to deduce the mass of a star by its absolute visual magnitude is presented; the mass of a galaxy is deduced by analogy. In the case of the galaxies, the bolometric correction of the stars will be replaced by the sun's absolute magnitude and mass-luminosity ratio different in each selected band.

5.1. The case of the stars

In the case of the stars it is possible to parameterise the mass of the star, \mathcal{M}_S , as a function of the observable colour $(B-V)$, see Zaninetti (2005). The first equation connects the $(B-V)$ colour with the temperature

$$(B-V) = K_{BV} + \frac{T_{BV}}{T} , \quad (42)$$

here T is the temperature, K_{BV} and T_{BV} are two parameters that can be derived by implementing the least square method on a series of calibrated data. The second equation

describes the bolometric correction , BC ,

$$BC = M_{\text{bol}} - M_V = -\frac{T_{\text{BC}}}{T} - 10 \log_{10} T + K_{\text{BC}} \quad , \quad (43)$$

where M_{bol} is the absolute bolometric magnitude, M_V is the absolute visual magnitude, T_{BC} and K_{BC} are two parameters that can be derived through the general linear least square method applied to a series of calibrated data. The third equation is the usual formula for the luminosity

$$\log_{10}\left(\frac{L}{L_{\odot}}\right) = 0.4(4.74 - M_{\text{bol}}) \quad , \quad (44)$$

where L is the luminosity of the star and L_{\odot} the luminosity of the sun. The fourth equation is the usual mass-luminosity relationship for stars

$$\log_{10}\left(\frac{L}{L_{\odot}}\right) = a_{\text{LM}} + b_{\text{LM}} \log_{10}\left(\frac{\mathcal{M}_S}{\mathcal{M}_{\odot}}\right) \quad (45)$$

for $\mathcal{M} > 0.2\mathcal{M}_{\odot}$,

where \mathcal{M}_S is the mass of the star and \mathcal{M}_{\odot} is the mass of the sun.

With these four equations the mass of the star is

$$\log_{10} \frac{\mathcal{M}_S}{\mathcal{M}_{\odot}} = \frac{-0.4 M_V - 0.4 K_{\text{BC}} + 4.0 \ln \left(\frac{T_{\text{BV}}}{(B-V) - K_{\text{BV}}} \right) (\ln(10))^{-1}}{b_{\text{LM}}} - \frac{0.4 \frac{T_{\text{BC}} (-(B-V) + K_{\text{BV}})}{T_{\text{BV}}} + 1.896 - a_{\text{LM}}}{b_{\text{LM}}} \quad , \quad (46)$$

with the various coefficients as given by Table 1 in Zaninetti (2005). As an example, the mass of a star belonging to MAIN SEQUENCE V is

$$\log_{10} \frac{\mathcal{M}_S}{\mathcal{M}_{\odot}} = -7.769 + 0.8972 \ln \left(\frac{7361}{(B-V) + 0.6411} \right) \quad . \quad (47)$$

We can now express the colour $(B-V)$ as a function of the absolute visual magnitude M_V and the following formula for the mass of the star is obtained

$$\log_{10} \frac{\mathcal{M}_S}{\mathcal{M}_{\odot}} = -7.769 + 0.8972 \ln \left(\frac{9378}{W (9378 e^{-8.496+0.2972 M_V})} \right) \quad (48)$$

MAIN SEQUENCE V when $-5.8 < M_V < 11.8$,

where W is the Lambert W-function, after Lambert (1758). A test of the previous formula can be done at the two boundaries: when $M_V = -0.58$, $\log_{10} \frac{\mathcal{M}_S}{\mathcal{M}_\odot} = 1.63$ against the calibrated value $\log_{10} \frac{\mathcal{M}_S}{\mathcal{M}_\odot} = 1.6$ and when $M_V = 11.8$, $\log_{10} \frac{\mathcal{M}_S}{\mathcal{M}_\odot} = -0.56$ against the calibrated value $\log_{10} \frac{\mathcal{M}_S}{\mathcal{M}_\odot} = -0.66$, see Table 3.1 in Bowers & Deeming (1984).

5.2. The case of the galaxies

The mass of a galaxy can be evaluated once the mass luminosity ratio, R is given

$$R = \left\langle \frac{M}{L} \right\rangle \quad . \quad (49)$$

Some values of R are now reported : $R \leq 20$ by Kiang (1961) and Persic & Salucci (1992), $R = 20$ by Padmanabhan (1996), $R = 5.93$ by van der Marel (1991). Further on Bell & de Jong (2001), demonstrated (amongst others) that $\frac{\mathcal{M}}{L}$ varies as a function of galaxy colour, and therefore, type. If the bright end of the luminosity function is dominated by massive, evolved, red galaxies, and the faint end by low mass, blue galaxies, then $\frac{\mathcal{M}}{L} \propto L^{-0.64}$ (GIANTS III) at the bright end and $\frac{\mathcal{M}}{L} \propto L^{-0.7}$ (MAIN SEQUENCE V) at the faint end, see coefficients of Table 1 in Zaninetti (2005). Then $\frac{\mathcal{M}}{L}$ will almost certainly not be constant due to different prevailing populations of stars at the boundaries of the luminosity function. The scatter in the models by Bell & de Jong (2001) is a starting point when evaluating the validity of assuming a constant $\frac{\mathcal{M}}{L}$. Generally, near-infrared $\frac{\mathcal{M}}{L}$ ratios are more constant than optical passband, but still vary with luminosity. In our framework, we made R a function of the passband, in order to have the same results for the masses of the galaxies once the absolute magnitude is given, see Figure 15. In our framework R can be expressed as

$$R = \frac{\langle \mathcal{M} \rangle}{\langle L \rangle} \quad . \quad (50)$$

On inserting formula (14) and formula (20) in the previous ratio the following formula for \mathcal{M}^* is found

$$\mathcal{M}^* = RL^* \frac{\Gamma(c+a)}{\Gamma(c)} \frac{\mathcal{M}_\odot}{L_\odot} \quad . \quad (51)$$

From equations (15) and (51) a formula for the mass of the galaxy is found

$$\mathcal{M} = \frac{R 10^{(0.4 M_{bol,\odot} - 0.4 M^*)} \Gamma(c+a) (10^{-0.4 M + 0.4 M^*})^{a-1}}{c \Gamma(c)} \mathcal{M}_\odot \quad . \quad (52)$$

An application of the previous formula is reported in Figure (15), where the mass of galaxies as a function of the absolute magnitude in the five bands of SDSS is drawn. In

this Figure $M_{bol,\odot}$ is different for each selected band and equal to the value suggested in equation (16) of Blanton et al. (2001).

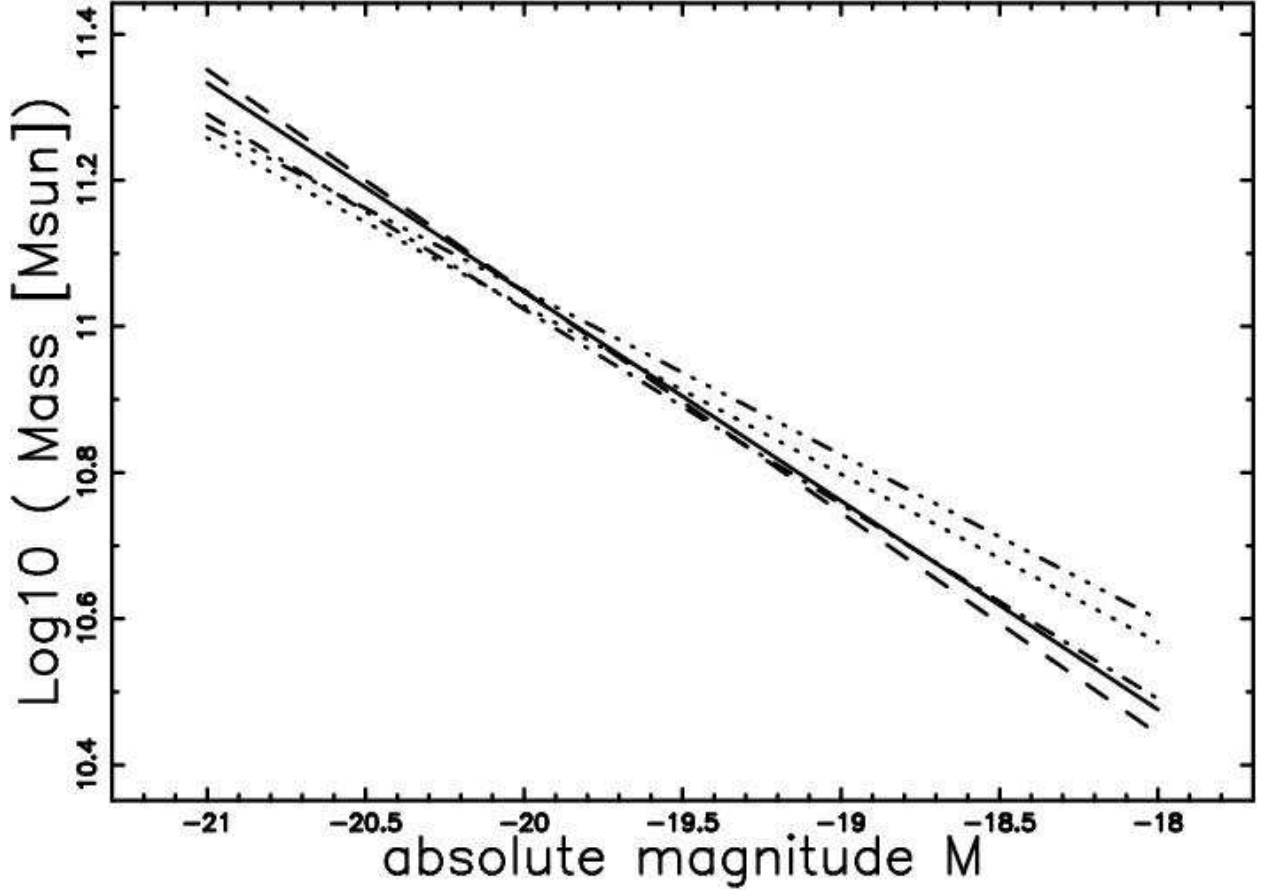


Fig. 15.— Logarithm of the mass of the galaxy as a function of the absolute magnitude. The SDSS bands are u^* with $M_{bol,\odot}=M_{u^*\odot}=6.39$ and $R = 6$ (full line) , g^* with $M_{bol,\odot}=M_{g^*\odot}=5.07$ and $R = 13$ (dashed), r^* with $M_{bol,\odot}=M_{r^*\odot}=4.62$ and $R = 16$ (dot-dash-dot-dash), i^* with $M_{bol,\odot}=M_{i^*\odot}=4.52$ and $R = 15$ (dotted), z^* with $M_{bol,\odot}=M_{z^*\odot}=4.48$ and $R = 14$ (dash-dot-dot-dot).

The new formula (52) allows us to deduce the mass of the galaxy from its absolute magnitude and can be easily particularized in different pass-bands. As an example , with the data of SDSS in the five bands reported in Table 2 , $M_{bol,\odot}$ as in equation (16) of Blanton et al. (2001) and R as in Figure 15, we have

$$\begin{aligned}
 \mathcal{M} &= 215234 e^{-0.6579 M} \mathcal{M}_{\odot} & u^* \text{ band when } -20.6 \leq M \leq -15.7 \\
 \mathcal{M} &= 97216 e^{-0.6978 M} \mathcal{M}_{\odot} & g^* \text{ band when } -22.0 \leq M \leq -18.2 \\
 \mathcal{M} &= 490000 e^{-0.6141 M} \mathcal{M}_{\odot} & r^* \text{ band when } -23.0 \leq M \leq -19 \\
 \mathcal{M} &= 2691000 e^{-0.5294 M} \mathcal{M}_{\odot} & i^* \text{ band when } -23.5 \leq M \leq -19.3 \\
 \mathcal{M} &= 3434000 e^{-0.5175 M} \mathcal{M}_{\odot} & z^* \text{ band when } -23.7 \leq M \leq -20.0 \quad .
 \end{aligned} \tag{53}$$

The method here suggested to deduce the mass of the galaxy can be compared with the formula that comes out from the Tully-Fisher relation , see Tully & Fisher (1977) and Tully et al. (1998). In the Tully-Fisher framework the mass of a rotating galaxy can be parameterised as

$$\mathcal{M} = 50 V_f^4 \mathcal{M}_{\odot} \frac{s^4}{K m^4} \quad , \tag{54}$$

where V_f is the rotational velocity expressed in $\frac{Km}{s}$, see McGaugh (2005). The mass to light ratio in our framework scales $\propto L^{(1/a)-1}$ with a depending on the selected catalog and band. This ratio oscillates , referring to the SDSS data, between a minimum dependence in the g^* band , $\frac{\mathcal{M}}{L} \propto L^{-0.24}$ and a maximum dependence in the i^* band , $\frac{\mathcal{M}}{L} \propto L^{-0.42}$. A comparison should be made with $\frac{\mathcal{M}}{L} \propto L^{0.35}$ in van der Marel (1991) for a sample of 37 bright elliptical galaxies ; this result was obtained by implementing axisymmetric dynamical models. The completeness of the mass sample of the galaxies belonging to a given catalog can be evaluated in the following way. The limiting apparent magnitude is known, and is different for each catalog. In the case of the SDSS (r^* band) is $m=17.6$, see Blanton et al. (2001).

The corresponding absolute limiting magnitude is computed and inserted in equation (52). The limiting mass for galaxies , \mathcal{M}_L ,is

$$\mathcal{M}_L = R \frac{10^{(0.4 M_{bol,\odot} - 0.4 M^*)} \Gamma(c+a) \left(10^{-0.4 m + 2.0 \text{Log} 10 \left(\frac{c_L z}{H_0} \right) + 10.0 + 0.4 M^*} \right)^{a-1}}{c (\Gamma(c))} \mathcal{M}_{\odot} \quad , \tag{55}$$

where $c_L z$ is the radial distance expressed in km/s . In order to see how the parameter z influences the limiting mass, Table 7 reports the range of observable masses as a function of z .

6. Conclusions

We have split the analysis of the luminosity function in two . The analysis of the main new luminosity function , formula (18), from low luminosities up to maximum magnitude shows that , see Table 2,

1. The parameter c varies between 0.1 and 2. It must be remembered that the theory predicts 2 , 4 and 6 for the 1D,2D and 3D fragmentation respectively.
2. Parameter a varies between 1.32 and 1.74. The numerical mass-luminosity relationship for the stars gives values of the parameter a comprised between 2.43 and 3.43.
3. The $\mathcal{M} - L$ function represents a better fit of the observational data in comparison with the Schechter function once the concept of maximum magnitude of the sample is introduced. Without this limiting magnitude the situation is inverted.

The case of low luminosities galaxies was describe by a truncated Pareto type luminosity function , see formula (29). This new luminosity function is described by two physical parameters , d , and a denoting respectively the distribution in mass and the mass-luminosity connection. The analysis of the data for low luminosities galaxies as reported in Table 3 shows that

1. The parameter d varies between 0.3 and 0.9 . This value should be compared with d of the stars which is $2.3 - 1 = 1.3$, see Kroupa (2001).
2. The parameter a varies between 1.3 and 2.7.

Table 7: The limiting mass for the SDSS catalog , u^* band, when R and $M_{bol,\odot}$ are those of Figure 15. The limiting apparent magnitude is $m=17.6$.

<i>mass range</i>	<i>z</i>
$1.4110^8 \mathcal{M}_{\odot} < \mathcal{M} < 1.7 \cdot 10^{11} \mathcal{M}_{\odot}$	0.001
$3.7910^9 \mathcal{M}_{\odot} < \mathcal{M} < 1.7 \cdot 10^{11} \mathcal{M}_{\odot}$	0.01
$1.010^{11} \mathcal{M}_{\odot} < \mathcal{M} < 1.7 \cdot 10^{11} \mathcal{M}_{\odot}$	0.1
$1.410^{11} \mathcal{M}_{\odot} < \mathcal{M} < 1.7 \cdot 10^{11} \mathcal{M}_{\odot}$	0.13

The theoretical number of galaxies as a function of the red-shift presents a maximum that is a function of α and f for the Schechter function and c , a and f for the first $\mathcal{M} - L$ function ; the agreement with the maximum in the observed number of galaxies is acceptable.

The observable range in masses can be parameterised as a function of z and the ratio between maximum and minimum luminosity is 232 at $z=0.001$ but drops to 1.1 at $z=0.15$, see Table 7.

Perhaps a more comprehensive way of comparing the mass estimates of equation (54) (Tully-Fisher relation) with those given here (equation (52) and equation (53)) would be as follows. We take the same sample of galaxies for which the luminosity function was computed in Section 3 and compute their mass function according to a given value of R . This mass function can be compared with those of other galaxies in a common passband and, also in this case, the distribution is expressed through a Schechter function. Three cases are now analysed

1. The Bell case , see Bell et al. (2003a), where $\Phi^* = 0.01 Mpc^{-3}/Log_{10}(\mathcal{M})$, $\mathcal{M}^* = 5.3 \cdot 10^{10} \mathcal{M}_{\odot}$ and $\alpha = -1.21$.
2. The Bottema case , see Bottema (1997), where $\Phi^* = 0.014 Mpc^{-3}/Log_{10}(\mathcal{M})$, $\mathcal{M}^* = 2.24 \cdot 10^{10} \mathcal{M}_{\odot}$ and $\alpha = -1.20$.
3. Kennicutt-Kroupa case , see Kennicutt (1983); Kroupa et al. (1993), where $\Phi^* = 0.011 Mpc^{-3}/Log_{10}(\mathcal{M})$, $\mathcal{M}^* = 3.78 \cdot 10^{10} \mathcal{M}_{\odot}$ and $\alpha = -1.22$.

Figure 16 reports the already cited standard distributions as well as our $\Psi(\mathcal{M})/Log_{10}(\mathcal{M})$ when the range in masses is that given by the conversion from luminosity to masses.

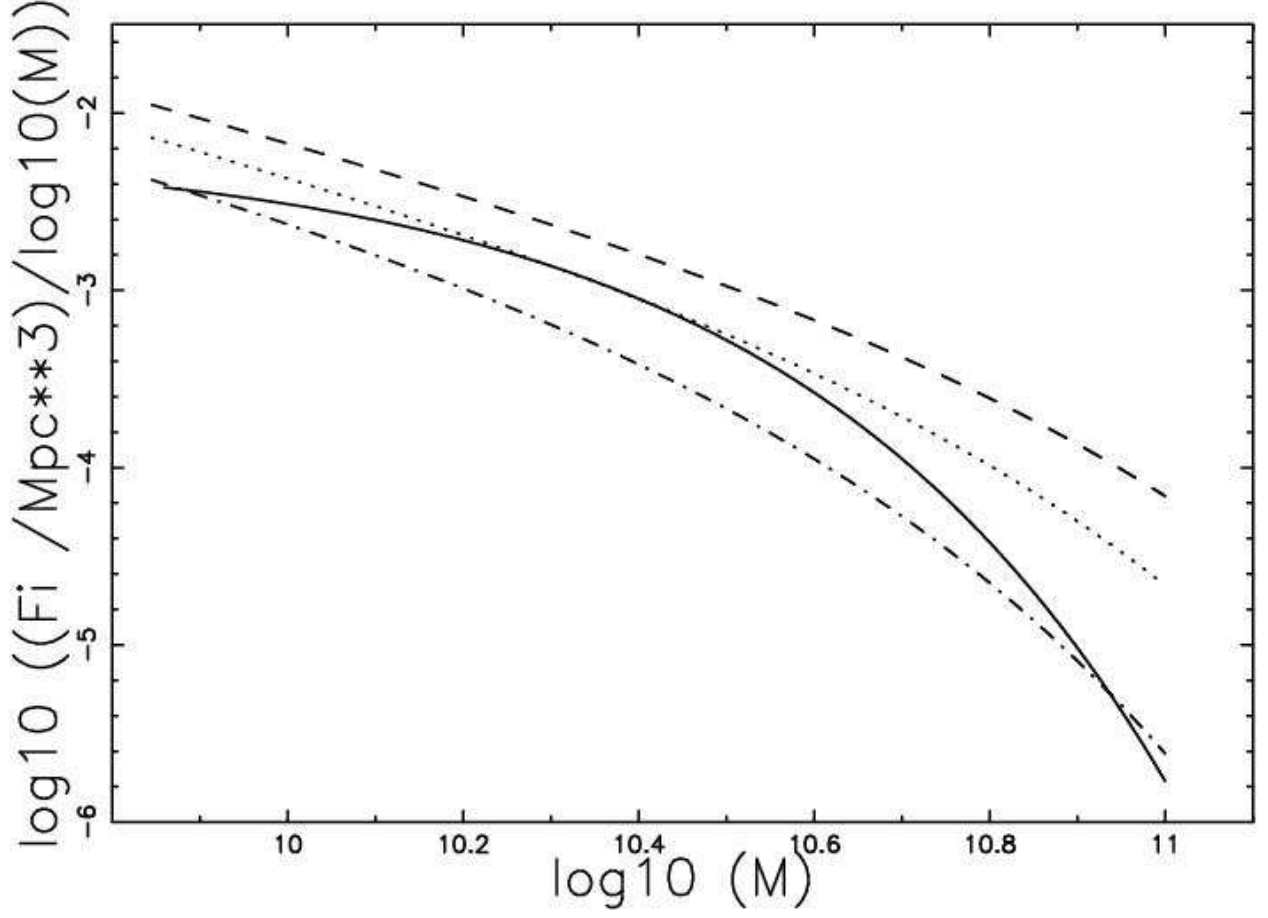


Fig. 16.— Barionic Mass function of galaxies: our $\Psi(\mathcal{M})/Log_{10}(\mathcal{M})$ (full line) , Bell case (dashed), Bottema case (dot-dash-dot-dash) and Kennicutt-Kroupa case (dotted). In our case we considered the SDSS band u^* with $M_{bol,\odot}=M_{u^*,\odot}=6.39$ and $R=6.0$.

The analysis of the two new functions for the luminosity for galaxies here derived gives a marginally better fit but certainly the Schechter function for its simplicity and fewer parameters still represents a good model for the luminosity function for galaxies. At present the study of the Schechter function is not yet terminated and two new equations were derived: equation (3) that represents the maximum in magnitude distribution and equation (33) that gives the value of z at which the observed number of galaxies is maximum.

A. On the Kiang Function

The starting point is the distribution in length, s , of a segment in a random fragmentation

$$p(s) = \lambda \exp(-\lambda s) ds \quad , \quad (\text{A1})$$

where λ is the hazard rate of the exponential distribution. Given the fact that the sum, u , of two exponential distributions is

$$p(u) = \lambda^2 u \exp(-\lambda u) du \quad . \quad (\text{A2})$$

The distribution of 1D Voronoi segments, l , (the midpoint of the sum of two segments) can be found from the previous formula by inserting $u = 2l$

$$p(l) = 2\lambda l \exp(-2\lambda l) d(2\lambda l) \quad . \quad (\text{A3})$$

On transforming in normalised units $x = \frac{l}{\lambda}$ we obtain

$$p(x) = 2x \exp(-2x) d(2x) \quad . \quad (\text{A4})$$

After one century of studies on the Voronoi diagrams, see the two memories Voronoi (1907) and Voronoi (1908), the law of the segments in 1D is the unique analytical result on the field. When this result is expressed as a gamma variate we obtain formula(5) of Kiang (1966)

$$H(x; c) = \frac{c}{\Gamma(c)} (cx)^{c-1} \exp(-cx) \quad , \quad (\text{A5})$$

where $0 \leq x < \infty$, $c > 0$ and $\Gamma(c)$ is the gamma function with argument c ; in the case of 1D Voronoi diagrams $c = 2$. It was conjectured that the area in 2D and the volumes in 3D of the Voronoi diagrams may be approximated as the sum of two and three gamma variate of argument 2. Due to the fact that the sum of n independent gamma variates with shape parameter c_i is a gamma variate with shape parameter $c = \sum_i^n c_i$, the area and the volumes are supposed to follow a gamma variate of argument 4 and 6. This hypothesis was later named "Kiang's conjecture", and the equation (A5) used as a fitting function,

see Kumar et al. (1992); Zaninetti (2006), or as an hypothesis to accept or to reject using the standard procedures of the data analysis, see Tanemura (1988, 2003). A new way to parametrise the 1D, 2D and 3D cells on the base of the considered dimensionality has been introduced , see formula (12) in Ferenc & Néda (2007).

B. On the Truncated Pareto Distribution

The starting pdf (probability density function) is the Pareto distribution Pareto (1896); Evans et al. (2000), P,

$$P(x; a, c) = \frac{ca^c}{x^{c+1}} \quad , \quad (\text{B1})$$

where $a \leq x < \infty$, $a > 0$, $c > 0$. The average value is

$$\bar{x} = \frac{ca}{c-1} \quad , \quad (\text{B2})$$

which is defined for $c > 1$, and the variance is

$$\sigma^2 = \frac{a^2c}{(c-2)(c-1)^2} \quad , \quad (\text{B3})$$

which is defined for $c > 2$. The presence of an upper bound , b , allows us to introduce the following pdf , named truncated Pareto P_T ,

$$P_T(x; a, b, c) = \frac{1}{1 - (\frac{a}{b})^c} \frac{ca^c}{x^{c+1}} \quad , \quad (\text{B4})$$

here $a \leq x \leq b$, $a > 0$, $b > 0$, $b > a$ and $c > 0$. The distribution function of the truncated Pareto is

$$F(x; a, b, c) = \frac{1 - (\frac{a}{x})^c}{1 - (\frac{a}{b})^c} \quad . \quad (\text{B5})$$

The average value of the truncated Pareto pdf is

$$\bar{x} = \frac{ca}{c-1} \frac{1 - (\frac{a}{b})^{c-1}}{1 - (\frac{a}{b})^c} \quad , \quad (\text{B6})$$

and the variance of the truncated Pareto pdf is

$$\sigma^2 = \frac{\text{numerator}}{\text{denominator}} \quad , \quad (\text{B7})$$

with

$$\text{denominator} = (c-2)(c-1)^2 (a^{2c} - 2b^c a^c + b^{2c}) \quad , \quad (\text{B8})$$

$$\begin{aligned} \text{numerator} = \\ cb^2a^{2c} + 2a^{2+c}c^2b^c - 4c^2a^{c+1}b^{c+1} + 2c^2b^{2+c}a^c - a^{2+c}cb^c \\ + 2c^3a^{c+1}b^{c+1} - a^{2+c}c^3b^c - c^3b^{2+c}a^c - cb^{2+c}a^c + ca^2b^{2c} \end{aligned}$$

The variance of the truncated Pareto is always defined for every value of $c > 0$; conversely the variance of the Pareto distribution can be defined only when $c > 2$. The parameter c can be derived through the maximum likelihood estimator (MLE). The likelihood function is defined as the probability we would have obtained a given set of observations if given a particular set of values of the distribution parameters, c_i ,

$$L(c) = f(x_1 \dots x_n | c_1 \dots c_n) \quad . \quad (\text{B9})$$

If we assume that the n random variables are independently and identically distributed, then we may write the likelihood function as

$$L(c) = f(x_1 | c_1 \dots c_p) \dots f(x_n | c_1 \dots c_p) = \prod_{i=1}^n f(x_i | c_1 \dots c_p) \quad . \quad (\text{B10})$$

The maximum likelihood estimates for the c_i are obtained by maximising the likelihood function, $L(c)$. Equivalently, we may find it easier to maximise $\ln f(x_i)$, termed the log-likelihood. So, for a random sample $x_1 \dots x_n$ from a truncated Pareto distribution, the likelihood function is given by

$$L(c) = \prod_{i=1}^n c \left((a^c)^{-1} - (b^c)^{-1} \right)^{-1} (x_i^{c+1})^{-1} \quad . \quad (\text{B11})$$

In this model we have assumed that $a = \min(x_1 \dots x_n)$ and $b = \max(x_1 \dots x_n)$.

Using logarithms, we obtain the log-likelihood

$$\ln L(c) = nc \ln(a) + n \ln \frac{c}{1 - (\frac{a}{b})^c} - \sum_{i=1}^n \ln x_i \quad . \quad (\text{B12})$$

Taking the first derivative, we get

$$\begin{aligned} \frac{\partial}{\partial c} \ln L(c) = 0 \\ n \ln a + \frac{n}{c} + \frac{n(\frac{a}{b})^c \ln(\frac{a}{b})}{1 - (\frac{a}{b})^c} - \sum_{i=1}^n \ln x_i = 0 \quad . \end{aligned} \quad (\text{B13})$$

The parameter c can be found by solving numerically the previous non-linear equation.

I thank Massimo Ramella, Tao Kiang and the anonymous referee for comments.

REFERENCES

- Aban, I., Meerschaert, M., & Panorska, A. 2006, *Journal of the American Statistical Association*, 101, 270
- Bell, E. F., & de Jong, R. S. 2001, *ApJ*, 550, 212
- Bell, E. F., McIntosh, D. H., Katz, N., & Weinberg, M. D. 2003a, *ApJ*, 585, L117
- . 2003b, *ApJS*, 149, 289
- Binney, J., & Merrifield, M. 1998, *Galactic astronomy* (Princeton, NJ: Princeton University Press)
- Blanton, M. R., Dalcanton, J., Eisenstein, D., Loveday, J., Strauss, M. A., SubbaRao, M., Weinberg, D. H., Anderson, J. E., Annis, J., Bahcall, N. A., Bernardi, M., Brinkmann, J., & Brunner, R. J. 2001, *AJ*, 121, 2358
- Blanton, M. R., Hogg, D. W., Bahcall, N. A., Brinkmann, J., Britton, M., Connolly, A. J., Csabai, I., Fukugita, M., Loveday, J., Meiksin, A., Munn, J. A., Nichol, R. C., Okamura, S., Quinn, T., Schneider, D. P., Shimasaku, K., Strauss, M. A., Tegmark, M., Vogeley, M. S., & Weinberg, D. H. 2003, *ApJ*, 592, 819
- Blanton, M. R., Lupton, R. H., Schlegel, D. J., Strauss, M. A., Brinkmann, J., Fukugita, M., & Loveday, J. 2005, *ApJ*, 631, 208
- Bottema, R. 1997, *A&A*, 328, 517
- Bowers, R. L., & Deeming, T. 1984, *Astrophysics. I and II* (Boston: Jones and Bartlett)
- Burroughs, S. M., & Tebbens, S. F. 2001, *Pure and Applied Geophysics*, 158, 741
- Charlton, J. C., & Schramm, D. N. 1986, *ApJ*, 310, 26
- Cohen, A., & Whitten, B. 1988, *Parameter Estimation in reliability and Life Span Models* (New York: Marcel Dekker)
- Cox, A. N. 2000, *Allen’s astrophysical quantities* (New York: Springer)
- Cross, N., Driver, S. P., Couch, W., Baugh, C. M., Bland-Hawthorn, J., Bridges, T., Cannon, R., Cole, S., Colless, M., Collins, C., Dalton, G., Deeley, K., De Propriis, R., Efstathiou, G., Ellis, R. S., Frenk, C. S., Glazebrook, K., Jackson, C., Lahav, O., Lewis, I., Lumsden, S., Maddox, S., Madgwick, D., Moody, S., Norberg, P., Peacock, J. A., Peterson, B. A., Price, I., Seaborne, M., Sutherland, W., Tadros, H., & Taylor, K. 2001, *MNRAS*, 324, 825

- Devoto, D., & Martnez, S. 1998, *Mathematical Geology*, 30, 661
- Dicenzo, S. B., & Wertheim, G. K. 1989, *Phys. Rev. B*, 39, 6792
- Driver, S. P., Liske, J., Cross, N. J. G., De Propriis, R., & Allen, P. D. 2005, *MNRAS*, 360, 81
- Driver, S. P., & Phillipps, S. 1996, *ApJ*, 469, 529
- Drouffe, J. M., & Itzykson, C. 1984, *Nuclear Physics B*, 235, 45
- Elmegreen, B. G. 2004, *MNRAS*, 354, 367
- Evans, M., Hastings, N., & B., P. 2000, *Statistical Distributions - third edition* (New York: John Wiley & Sons Inc)
- Ferenc, J.-S., & Nédá, Z. 2007, *Physica A Statistical Mechanics and its Applications*, 385, 518
- Hentschel, H. G. E., Ilyin, V., Makedonska, N., Procaccia, I., & Schupper, N. 2007, *Phys. Rev. E*, 75, 050404
- Jerauld, G. R., Hatfield, J. C., Scriven, L. E., & Davis, H. T. 1984a, *Journal of Physics C Solid State Physics*, 17, 1519
- Jerauld, G. R., Scriven, L. E., & Davis, H. T. 1984b, *Journal of Physics C Solid State Physics*, 17, 3429
- Jones, D. H., Peterson, B. A., Colless, M., & Saunders, W. 2006, *MNRAS*, 369, 25
- Kennicutt, Jr., R. C. 1983, *ApJ*, 272, 54
- Keres, D., Yun, M. S., & Young, J. S. 2003, *ApJ*, 582, 659
- Kiang, T. 1961, *MNRAS*, 122, 263
- . 1966, *Zeitschrift fur Astrophysics*, 64, 433
- Kroupa, P. 2001, *MNRAS*, 322, 231
- Kroupa, P., Tout, C. A., & Gilmore, G. 1993, *MNRAS*, 262, 545
- Kumar, S., Kurtz, S. K., Banavar, J. R., & M.G., S. 1992, *Journal of Statistical Physics*, 67, 523

- Lambert, J. H. 1758, *Acta Helvetica, physico-mathematico-anatomico-botanico-medica*, 3, 128
- Lang, K. R. 1999, *Astrophysical formulae* (New York: Springer)
- Lee, T.-Y., & Chen, J. S. 2006, *International Journal for Computational Methods in Engineering Science and Mechanics*, 7, 475
- Lin, H., Kirshner, R. P., Shectman, S. A., Landy, S. D., Oemler, A., Tucker, D. L., & Schechter, P. L. 1996, *ApJ*, 464, 60
- Madgwick, D. S., Lahav, O., Baldry, I. K., Baugh, C. M., Bland-Hawthorn, J., Bridges, T., Cannon, R., Cole, S., Colless, M., Collins, C., Couch, W., Dalton, G., De Propriis, R., Driver, S. P., Efstathiou, G., Ellis, R. S., Frenk, C. S., Glazebrook, K., Jackson, C., Lewis, I., Lumsden, S., Maddox, S., Norberg, P., Peacock, J. A., Peterson, B. A., Sutherland, W., & Taylor, K. 2002, *MNRAS*, 333, 133
- McGaugh, S. S. 2005, *ApJ*, 632, 859
- Okabe, A., Boots, B., & Sugihara, K. 1992, *Spatial tessellations. Concepts and Applications of Voronoi diagrams* (Chichester, New York: Wiley)
- Padmanabhan, T. 1996, *Cosmology and Astrophysics through Problems* (Cambridge: Cambridge University Press)
- Pareto, V. 1896, *Cours d’ economie politique* (Lausanne: Rouge)
- Persic, M., & Salucci, P. 1992, *MNRAS*, 258, 14P
- Press, W. H., Teukolsky, S. A., Vetterling, W. T., & Flannery, B. P. 1992, *Numerical recipes in FORTRAN. The art of scientific computing* (Cambridge: Cambridge University Press)
- Rehfeldt, K., Boggs, J. M., & Gelhar, L. W. 1992, *Water Resour. Res.*, 28, 3309
- Salpeter, E. E. 1955, *ApJ*, 121, 161
- Scalo, J. M. 1986, *Fundamentals of Cosmic Physics*, 11, 1
- Schechter, P. 1976, *ApJ*, 203, 297
- Tanemura, M. 1988, *J. Microscopy*, 151, 247
- . 2003, *Forma*, 18, 221

- Tully, R. B., & Fisher, J. R. 1977, *A&A*, 54, 661
- Tully, R. B., Pierce, M. J., Huang, J.-S., Saunders, W., Verheijen, M. A. W., & Witchalls, P. L. 1998, *AJ*, 115, 2264
- van der Marel, R. P. 1991, *MNRAS*, 253, 710
- Voronoi, G. 1907, *Z. Reine Angew. Math*, 133, 97
- . 1908, *Z. Reine Angew. Math*, 134, 198
- Zaninetti, L. 2005, *Astronomische Nachrichten*, 326, 754
- . 2006, *Chinese J. Astron. Astrophys.*, 6, 387
- Zaninetti, L., & Ferraro, M. 1990, *A&A*, 239, 1